EFFECT OF TEMPORAL ACQUISITION PARAMETERS ON THE IMAGE QUALITY OF ULTRASOUND AXIAL STRAIN TIME-CONSTANT ELASTOGRAMS

A Thesis

by

JOSHUA KAVUNKAL VARGHESE

Submitted to the Office of Graduate Studies of
Texas A&M University
in partial fulfillment of the requirements for the degree of

MASTER OF SCIENCE

August 2011

Major Subject: Electrical Engineering

Effect of Temporal Acquisition Parameters on the Image Quality of Ultrasound Axial Strain Time-constant Elastograms

EFFECT OF TEMPORAL ACQUISITION PARAMETERS ON THE IMAGE QUALITY OF ULTRASOUND AXIAL STRAIN TIME-CONSTANT ELASTOGRAMS

A Thesis

by

JOSHUA KAVUNKAL VARGHESE

Submitted to the Office of Graduate Studies of
Texas A&M University
in partial fulfillment of the requirements for the degree of

MASTER OF SCIENCE

Approved by:

Chair of Committee,	Raffaella Righetti
Committee Members,	Jim Ji
	Deepa Kundur
	Riccardo Bettati
Head of Department,	Costas Georghiades

August 2011

Major Subject: Electrical Engineering

ABSTRACT

Effect of Temporal Acquisition Parameters on the Image Quality of Ultrasound Axial Strain Time-constant Elastograms. (August 2011)

Joshua Kavunkal Varghese, B.S., Texas A&M University

Chair of Advisory Committee: Dr. Raffaella Righetti

Recent developments in ultrasound elastography have suggested the possibility of using elastographic methods to estimate the temporal mechanical properties of complex tissues. In this context, elastographic methods to image the axial strain time constant (TC) have been developed. The axial strain TC is a parameter that is related to the viscoelastic and poroelastic behavior of tissues. Estimation of this parameter can be done using curve fitting methods. However, the effect of temporal ultrasonic acquisition parameters, such as window of observation, acquisition rate, and input noise, on the image quality of the resultant TC elastograms has not been investigated yet. Elucidating such effects could be useful for diagnostic applications.

This work explores the effects of varying windows of observation, acquisition rate, and input noise on the image quality (accuracy and signal-to-noise ratio (SNR)) of axial strain TC estimates and elastograms using a previously developed simulation model. By varying the amount of data collected as a percentage of the expected TC, the algorithms were able to compute a minimum threshold collection time for an accurate TC estimation as a percentage of the expected TC. The effect of acquisition parameters

such as acquisition rate and input noise on the minimum threshold collection time was assessed. Experimental data, collected for previous experiments, were used as a proof of principle to corroborate the simulation findings.

The results of this work suggest that there is a linear dependence of the total acquisition time necessary for accurate TC estimates on the true time constant value. The simulation results also indicate that it might be possible to make accurate estimates of the axial strain TC using small windows of observation (as small as 20% of the expected TC) with fast acquisition rates and high input SNR levels. Experimental results suggest that, in practice, a larger window of observation should be used to account for multiple noise sources typically not considered in simulations. This work also suggests that the minimum window of observation necessary for an accurate TC estimate is highly dependent on the acquisition frame rate and the input SNR level. Therefore, use of imaging systems with fast acquisition rates is recommended for studies aiming at measuring time-dependent phenomena in tissues.

ACKNOWLEDGEMENTS

I would like to thank my committee chair, Dr. Raffaella Righetti, for her patience, guidance, and support throughout the course of this research. I also want to thank my committee members, Dr. Ji, Dr. Kundur, and Dr. Bettati, for their help and support.

I want to extend my gratitude to the Texas A&M University Electrical and Computer Engineering department and the Texas A&M Supercomputing Facility for providing the facilities and support that helped make this work possible. Special thanks go to Sanjay Nair for his help in the simulation study and for providing the experimental data used in this study. I'd like to thank all my colleagues in the lab for their enormous patience with me.

Finally, thanks to my family and friends, whose constant love, support, and prayers have been a tremendous blessing in my life.

TABLE OF CONTENTS

Page

Page

LIST OF FIGURES

Page

Page

LIST OF TABLES

Page

CHAPTER I

INTRODUCTION

1. Introduction

Ultrasound elastography is a well-established non-invasive imaging modality which can be used to complement sonography and detect a variety of pathologies in soft tissues (Ophir et al. 1999; Itoh et al. 2006; Thomas et al. 2006; Thomas et al. 2007). Axial strain elastograms are the most commonly used elastographic images in clinical applications. These images show the strain tensor component along the axis of the transducer. Past work has shown that axial strain elastograms are highly correlated to changes in the underlying stiffness distribution of a tissue when a small compression is applied and the tissue behaves like a linearly elastic solid (Srinivasan et al. 2004). In certain tissues, elastographic parameters such as the axial strain experience temporal changes following application of a force. These temporal changes may be related to underlying pathologies within the tissue (Righetti et al. 2005a; Righetti et al. 2007a; Righetti et al. 2007b; Righetti et al. 2007c). This is the case, for example, in poroelastic and viscoelastic tissues. Poroelastic materials are modeled as consisting of a solid skeleton, or matrix, that is sponge-like, porous, permeable, and elastic with a fluid within the pores of the matrix (Konofagou et al. 2001). Viscoelastic materials are modeled as

---

This thesis follows the style of Ultrasound in Medicine and Biology.

consisting of an elastic spring component and a viscous dashpot component (Zhang 2005).

Application of poroelastography and viscoelasticity studies has led to the development of several new types of elastograms related to the poroelastic and viscoelastic behavior of tissues. Among these are the effective Poisson's ratio (EPR) elastogram, EPR time constant (TC) elastogram, and the axial strain TC elastogram, which is investigated in this work. These elastograms may potentially provide new information about tissues, which may be clinically useful for detection of pathologies and other physical conditions (Ammann et al. 2006; Righetti et al. 2007b; Qiu et al. 2008).

Previous work on axial strain TC elastography performed in our lab has led to the development of a real-time TC estimator for elastography applications (Nair et al. 2011). However, in TC elastography studies, ultrasonic data needs to be acquired for a certain amount of time (which depends on the true underlying tissue properties) before an elastogram can be created. The data acquisition process is the most time consuming portion of creating TC elastograms in clinical applications. Minimizing the time spent acquiring data would be beneficial for patients. No systematic study has been done to assess the acquisition requirements necessary to make accurate and reliable TC estimations. Since the TC acquisition process is not band-limited, standard sampling notions cannot be applied to predict the minimum window of observation (total acquisition time) that guarantees a TC estimate with a predefined level of accuracy. Therefore, this work aims to explore the effects of window of observation, acquisition

rate, and input noise on elastographic TC estimation. While these results specifically refer to ultrasound axial strain TC elastography, the findings reported in this thesis may be useful for general studies aiming at estimating the temporal mechanical behavior of tissues.

2. Objective and hypothesis

The objective of this work is to analyze the performance of an axial strain TC estimator under different windows of observation, acquisition rates, and noise levels. The hypothesis is that the window of observation required to obtain accurate estimates of the axial strain TC depends on the underlying tissue TC. I further hypothesize that it is possible to obtain accurate TC estimations even when using windows of observation significantly lower than the underlying TC, provided that sufficiently fast acquisition rates are used and the input signal-to-noise ratio (SNR) is least 10 dB.

3. Research plan

Design a simulation model for testing TC estimation with different acquisition parameters

A simulation model for axial strain and axial strain TC estimation was necessary to test how the accuracy of estimation was affected as acquisition parameters changed. The model required the ability to manipulate the acquisition rate, input noise, and window of observation used for creating axial strain curves, which are then used to estimate the axial strain TC.

Assess the effects of acquisition parameters on estimation accuracy

Analysis of the TC estimation process was performed to observe how the window of observation affected accuracy of estimates. Specifically, a threshold minimum window of observation for a given set of acquisition parameters was established. The threshold window of observation was defined as the smallest acquisition time necessary to consistently maintain a certain predefined level of accuracy in the TC estimates. Additionally, the effect of windows of observation smaller than this threshold on output image quality was studied. The effects of acquisition rate and input noise on the threshold window of observation were then assessed for multiple time constants, acquisition rates, and input SNR levels.

Corroborate simulation findings with experimental data

A process similar to the one employed for simulations was used to test how TC estimation of available experimental data was affected by the window of observation. Image quality was assessed statistically using standard evaluation factors.

4. Motivation

Faster diagnostics

A strong motivation at the basis of this work is the desire to shorten the time spent collecting ultrasound data for temporal elastographic experiments in clinical applications. Long data acquisition may be subjected to uncontrollable noise sources and may be uncomfortable for a patient. Obtaining information about the temporal

behavior of tissues quickly and accurately may allow faster diagnosis of diseases and medical conditions in patients. Maintaining a consistent quality level in the estimates while shortening acquisition time is also desirable for clinical applications.

Dependence of TC estimation on acquisition parameters

Past work has shown that the accuracy of TC estimates when using curve fitting methods depends on the curve fitting method used, the window of observation length, the sampling rate at which data are acquired, and the level of noise present in the data (Bendat and Piersol 1986; Nair et al. 2011). However, no study has elucidated the exact role of these parameters in TC estimation yet.

Justification for imaging systems with high frame rate

If imaging the temporal behavior of time-dependent phenomena in tissues is improved by using increased acquisition frame rates, then there may be a need to develop imaging systems that are capable of imaging at rates faster than those typically found in several clinical diagnostic systems. Therefore, state-of-the-art systems capable of acquiring at very fast frame rates may be useful for studies looking at time-dependent phenomena in tissues.

Applications to other types of elastograms and benefits for elastographic methods

The results of this work may be important for studies that deal with time-dependent phenomena in general. For example, the EPR of a material may also exhibit a

temporal change, allowing creation of EPR TC elastograms (Righetti et al. 2005a). Furthermore, it may be possible that these results may be applicable to other imaging modalities (for example, magnetic resonance imaging (MRI) or optical studies) focused on estimation of tissue temporal behaviors.

CHAPTER II

BASIC CONCEPTS

1. Elastography

The mechanical properties of tissues are dependent on many factors, including physiological and pathological factors (Ophir et al. 1999). Tissues are often assumed to behave as linearly elastic solids when subjected to a quasi-instantaneous compression (Ophir et al. 1999). Elastography techniques typically apply an external quasi-static compression to the tissue. The resulting local axial strains are estimated through cross-correlation analysis of pre- and post-compression echo signals (Ophir et al. 1991; Ophir et al. 1999). More recent developments in the field of elastography aim at imaging the temporal mechanical behavior of tissues. In these experiments, tissues may be subjected to a sustained compression by a constant axial compression force/stress (creep test) or by a constant axial strain (Chaudhry 2010; Nair 2010; Righetti et al. 2007b).

Elastographic techniques may be clinically useful in several types of medical applications, such as cancer imaging and the detection and staging of lymphedema (Righetti et al. 2007c; Berry et al. 2006; Berry et al. 2008). A number of studies have shown the usefulness of axial strain imaging of soft tissues, specifically of breast tissue, for determining the malignancy of potential tumors (Thomas et al. 2006; Thomas et al. 2007; Zhi et al. 2007; Itoh et al. 2006). The temporal behavior of tissues can also provide insight into underlying pathologies based on fluid content and mobility (Folkman 1992; Mridha and Ödman 1986). For example, Righetti et al. (2007c) have

suggested that axial strain elastograms, effective Poisson's ratio elastograms, and their corresponding time constant elastograms may provide valuable diagnostic information for distinguishing between normal and lymphedematous tissues.

Several elastographic techniques have been developed in recent years to image the temporal behavior of materials under mechanical loads or stresses (Konofagou et al. 2001; Righetti et al. 2005a). Among these are viscoelasticity imaging and poroelastography. Viscoelasticity imaging uses elastographic methods to observe time-dependent behavior in materials and tissue that can be modeled as viscoelastic (Sack et al. 2008; Liu and Ebbini 2008). Viscoelastic materials are often modeled as consisting of an elastic component and a viscous component. Following application of a stress, the strain experienced by a viscoelastic material depends on both components, which is often described by a combination of Hookean deformation and Newtonian flow patterns (Zhang 2005). Viscoelastic properties of tissues have been shown to correlate with pathological changes in stroma and connective tissues (Sridhar et al. 2007). Poroelastography is the use of elastographic techniques for imaging the temporal behavior of materials that can be modeled as poroelastic. Poroelastic materials are modeled as consisting of a solid skeleton, or matrix, that is sponge-like, porous, permeable, and elastic. Within the pores of this matrix is a fluid or gas. When a load is applied to the matrix, the pore fluid, which has a specific viscosity, can flow through the pores of the matrix at a rate depending on the permeability of the material (Berry et al. 2006; Konofagou et al. 2001). Permeability refers to the ease with which fluid can flow

through the pores in the material, and depends on the structure of the material, porosity, tortuosity, pore size, and pore interconnections (Collins 1961; Lu et al. 2009).

These two novel elastographic methods have led to the creation of several types of elastograms that may provide new information about the poroelastic and viscoelastic behavior of tissues. Among these are the effective Poisson's ratio (EPR) elastogram, the poroelastogram, and the axial strain TC elastogram. EPR is the ratio of lateral strain to axial strain, and describes how the volume of the material changes under load (Chaudhry 2010). A poroelastogram is defined as a series of EPR elastograms or axial strain elastograms, sequenced in time, obtained from a material under sustained axial compression. Poroelastograms have been shown to convey relevant information about the effective compressibility of the material being imaged (Righetti et al. 2004; Righetti et al. 2007a). When a poroelastic material is subjected to a constant compressive force (creep test), the EPR decays in time in an exponential manner as the fluid exits the matrix (Fortin et al. 2003; Righetti et al. 2007b). From the temporal behavior of the EPR, it is possible to create an EPR TC elastogram through curve-fitting. This elastogram may convey information about the permeability distribution of the poroelastic material (Righetti et al. 2007c; Righetti et al. 2005a).

Similarly, the axial strain and its temporal behavior may provide information about the viscoelastic and poroelastic properties of the material being imaged when creep or stress relaxation tests are performed (Righetti et al. 2007b; Ammann et al. 2006; Nair et al. 2011; Chaudhry 2010). Righetti et al. (2007b) showed the benefit of using axial strain elastography to distinguish differences in homogeneous poroelastic materials

with different elastic and permeability properties and for analysis of the time-dependent mechanical behavior of the materials. Qiu et al. (2008) reported the benefit of using viscoelastic retardation time constant estimation for discriminating between benign and malignant breast tumors, which have time constants smaller than 10 seconds. The work of Righetti et al. (2007c) reported EPR time constants on the order of hundreds of seconds and suggests that the temporal poroelastographic behavior of lymphedatous tissues may exhibit significant differences from the behavior that characterizes normal tissues.

2. Axial strain TC estimation

When a viscoelastic or poroelastic tissue is subjected to a constant force (creep), the axial strain experienced by the tissue changes with time. Several theoretical models can be used to extract relevant tissue time constants from the creep data (Samarin 1974; Fung 1981). The Kuei, Lai, and Mow biphasic theory has been used to predict time-dependent axial strain (Armstrong et al. 1984) and develop several theoretical models for poroelastography simulations (Konofagou et al. 2001; Berry et al. 2006). However, the model has not been applied directly to *in vivo* data, most likely due to its complexity.

Several studies have shown that simple exponential polynomials may serve as a suitable alternative for approximating creep data (Berry et al. 2006; Samarin 1974; Righetti et al. 2005a; Nair 2010). Models using a single exponential term have been used to study the temporal behavior of tissues (Nair et al. 2011; Righetti et al. 2005a; Qiu et al. 2008; Sridhar et al. 2007; Sridhar and Insana 2007). Analysis of these models

may be useful as a foundation for generalized models that use multiple exponential terms (Berry et al. 2006; Armstrong et al. 1984; Nair et al. 2011). A suitable model that has been used previously is given by (Nair et al. 2011):

$$S(t) = \eta + (\propto -\eta)e^{\frac{-t}{\tau}} \tag{2.1}$$

where *S(t)* is the axial strain at time t, η is the equilibrium axial strain at time t = ∞, α is the initial strain at time t = 0, and τ is the axial strain time constant. The two parameters of interest from this model that are typically unknown are the time constant τ and the equilibrium value η. These parameters are material-dependent and could be important for diagnostic purposes (Nair et al. 2011). In the absence of noise and if it was possible to collect data for an infinite amount of time, estimation of these parameters would be relatively simple.

In practice, it is only possible to acquire a limited series of noisy samples of the axial strain *S(t)* due to the discrete acquisition nature of the ultrasound system and various noise sources. A more accurate representation of the strain when using this model is then given by (Nair et al. 2011):

$$S(t_i) = \eta + (\propto -\eta)e^{\frac{-t_i}{\tau}} + N_i(t_i) \tag{2.2}$$

where $S(t_i)$ is a strain sample at time t_i, and $N_i(t_i)$ is a random variable modeled as a zero-mean Gaussian distribution.

In this model, the noise at each sample point $N_i(t_i)$ is assumed to come from a zero-mean Gaussian noise distribution. In this work, the axial strain curves from the model in (2.2) are assumed to have a constant signal-to-noise ratio (SNR) for the entire duration of the signal (Nair et al. 2011). The SNR is given by:

$$SNR(dB) = 20log_{10}(\frac{\mu_{signal}}{\sigma_{signal}}) \quad (2.3)$$

For a particular noisy strain sample, $\mu_{signal} = S(t_i)$ since $N_i(t_i)$ is zero-mean. Furthermore, $\sigma_{signal} = \sigma(N_i(t_i))$, since $N_i(t_i)$ is assumed to be the only source of variation for the signal (Nair 2010).

In practice, the calculation of a strain at a certain time during tissue compression must be done in a cumulative manner to minimize decorrelation noise due to uncontrollable physiological and subject motion (Nair et al. 2011; Righetti et al. 2005b). At each time, the strain can be computed as (Nair et al. 2011; Righetti et al. 2005b):

$$S(t_i) = S(t_{i-1}) + S(t_{i-1}, t_i) \quad (2.4)$$

Thus, the standard deviation of each strain is larger than the previous (in time) strain, since $\sigma(N_i(t_i)) > \sigma(N_{i-1}(t_{i-1}))$ (Nair 2010). The assumption of a constant SNR also means that smaller values of the signal $S(t_i)$ correspond to smaller values of the noise standard deviation $\sigma(N_i(t_i))$, which agrees with the nature of axial strain elastography (Nair 2010).

3. Strain estimation techniques

The behavior of the strain in (2.1) is quite similar to the voltage response of an RC circuit. A common approximation used in circuit theory is that the transient response of an RC circuit will reach equilibrium at approximately 5 times the time constant value (Nilsson and Riedel 2005). However, collecting correlated ultrasound data for a period of this length can be a significant challenge, especially in clinical applications.

The Nyquist-Shannon sampling theorem suggests that it is possible to fully reconstruct a band-limited signal by sampling at a frequency greater than twice the maximum frequency in the signal (Shannon 1949). However, it is possible to show that the temporal axial strain is not band-limited. For example, assume that the strain can be represented as:

$$S(t) = \left(\eta + (\propto -\eta)e^{\frac{-t}{\tau}}\right)u(t) \tag{2.5}$$

where *u(t)* is the unit step function, used to ensure that the application of the force occurs at time t = 0. The Fourier Transform of (2.5) is given by:

$$X(F) = \frac{\eta}{j2\pi F} + \eta\pi\delta(2\pi F) + \frac{\alpha-\eta}{\frac{1}{\tau}+j2\pi F} \tag{2.6}$$

The first and third terms in the resulting transform indicate that the signal is not band-limited. However, (2.6) suggests that it may be possible to improve accuracy of TC estimations by using faster acquisition rates.

Curve-fitting methods are often used to extract parameters of a model from a given set of data, and have been used in multiple elastography studies (Nair et al. 2011; Righetti et al. 2005a; Righetti et al. 2007b; Righetti et al. 2007c). Least-square error (LSE) curve fitting is a simple and common curve fitting technique that has been successfully used for parameter estimation (Nair et al. 2011; Cantrell 2008).

The work reported in this thesis uses the curve-fitting method developed by Nair et al. (2011). This estimator uses the Levenberg-Marquardt (LM) optimization algorithm to quickly find equation roots. The LM optimization algorithm is an iterative algorithm that uses gradient descent and the Newton method for finding equation roots,

and is useful for LSE minimization (Madsen et al. 2004; Nair et al. 2011). The algorithm has been successfully used in poroelastographic imaging in the past (Berry et al. 2006).

In the past, estimation of the time constant parameter τ has been done with little emphasis on the acquisition time or acquisition rate. This work looks to explore the effects of small windows of observation and fast acquisition rates on the estimation process. Figure 1 illustrates the concept at the basis of this work. This work looks to elucidate the accuracy of TC estimation when using different windows of observation, preferably window of observations shorter than the underlying TC. Three examples of data obtained using windows of observation shorter than the true TC are shown in Figure 1. Additionally, this work studies the effects of other acquisition parameters, such as acquisition rate and input noise, on TC estimation.

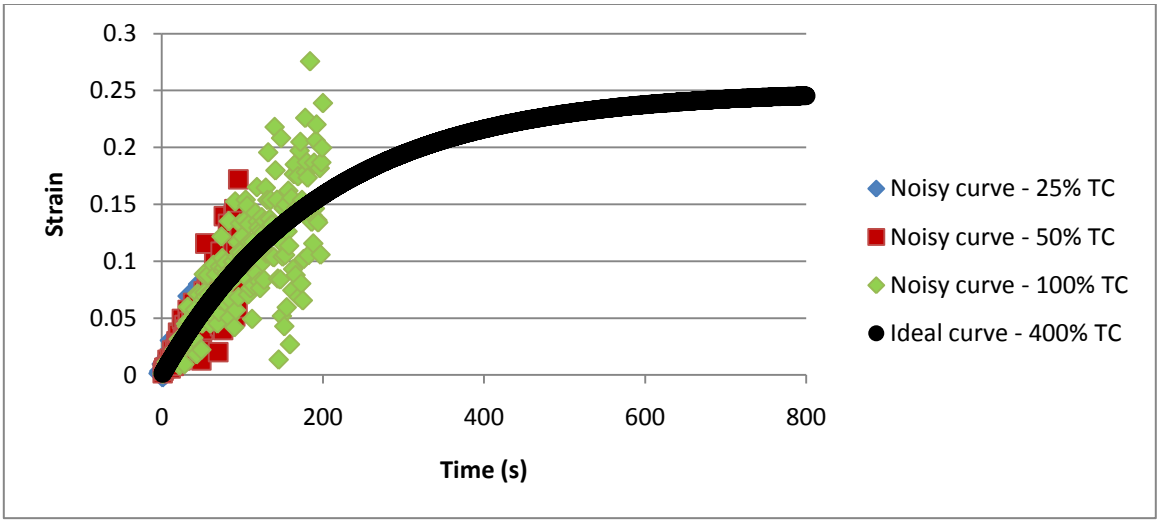

(a)

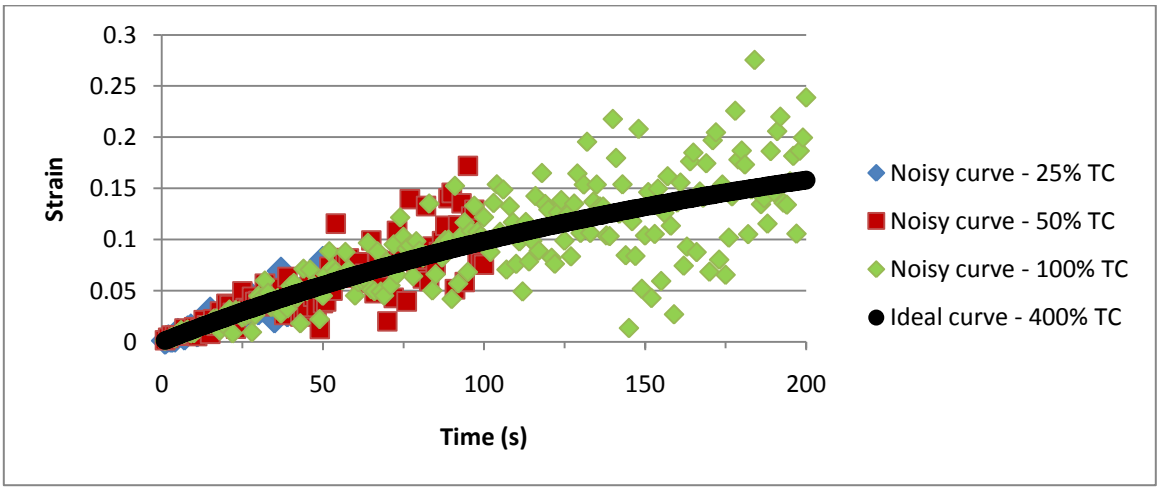

(b)

Figure 1. Simulated axial strain curves. TC value of 200s, 10dB input SNR, and 1 Hz acquisition rate. (a) Black curves show ideal axial strain curves collected for a window of observation equal to 400% of TC. Blue, red, and green curves show noisy strain curves for window of observations equal to 25%, 50%, and 100% of the true TC value. (b) Same curves in estimation range of interest.

CHAPTER III

SIMULATION METHODS AND RESULTS

This chapter describes the simulation methods used for analyzing image quality parameters and the effect of different temporal acquisition parameters.

1. Simulation methods

A simulation model using MATLAB was created to assess the effects of the temporal acquisition parameters on TC estimation accuracy (Nair et al. 2011). An overview of the simulation study used for TC estimation is described in Figure 2.

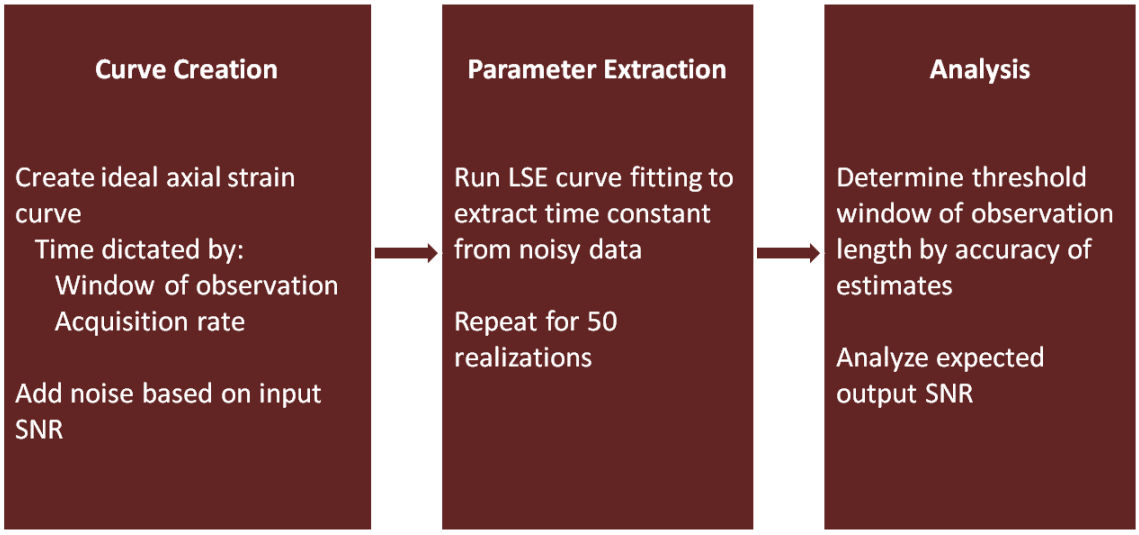

Figure 2. Simulation and statistical models used for a single TC.

The first step in the process is to create an ideal axial strain curve. The initial and equilibrium strain values, as well as the true TC, are assumed to be known. The total acquisition time used for each TC estimation is fixed by the desired window of observation, which is varied as a percentage of the underlying TC. The acquisition rate determines the number of samples used in each simulation. Once an ideal strain curve has been created, noise is added to the samples based on the input SNR used for the simulation. An in-house algorithm for least square error curve fitting method using Levenberg-Marquardt optimization is then used to estimate the axial strain TC for each window of observation. This process was repeated 50 times for a single TC and window of observation, providing 50 estimates of the true TC from noisy curves. The process of creating ideal curves, adding noise, and estimating the TC was repeated for multiple windows of observation for each TC. The threshold window of observation for a single TC was then determined by analyzing the accuracy of the TC estimates for all windows of observation tested. The threshold window of observation was defined as the smallest window of observation, given as a percentage of the true TC, such that, for all windows with a longer acquisition time, the accuracy of the LM estimator is always greater than 90%. Finally, output SNR achieved using the threshold window was analyzed to observe the expected quality levels. The entire process was repeated for multiple TC values.

The simulations used followed the creep model for ideal axial strain given by equation (2.2). Simulations assumed that the values for α, η, and τ are known prior to creation of the ideal strain curve. Additionally, the input SNR and acquisition rate are

fixed for each set of simulations. All simulations in this study used values of $\alpha = 0.0001$ and $\eta = 0.25$, which were used in previous work (Nair et al. 2011).

For a single TC, the window of observation for the ideal strain curve is varied in increments of 1% of the true TC. For example, for a true TC of 200 seconds and acquisition rate of 1 Hz, the first analyzed window of observation is equal to 1% of the TC, or 2 seconds total. The second window of observation is equal to 2% of the TC, or 4 seconds total, and so forth. The process is repeated up to a window of observation corresponding to 140% or 250% of the TC.

For a single TC and window of observation, Gaussian noise is added to the ideal curve. The amount of noise added is determined by the input SNR level. Figure 3 illustrates the effect of adding noise to an ideal strain curve with a TC of 200 seconds and 1 Hz acquisition rate such that the resultant noisy curve has a SNR of 10dB. Once noise has been added to an ideal curve for a specific TC and window of observation, the ideal curve is discarded, leaving only the noisy curve for TC estimation using the LM TC estimator developed by Nair et al. (2011). This process is repeated 50 times for each TC and window of observation, giving 50 TC estimates to analyze.

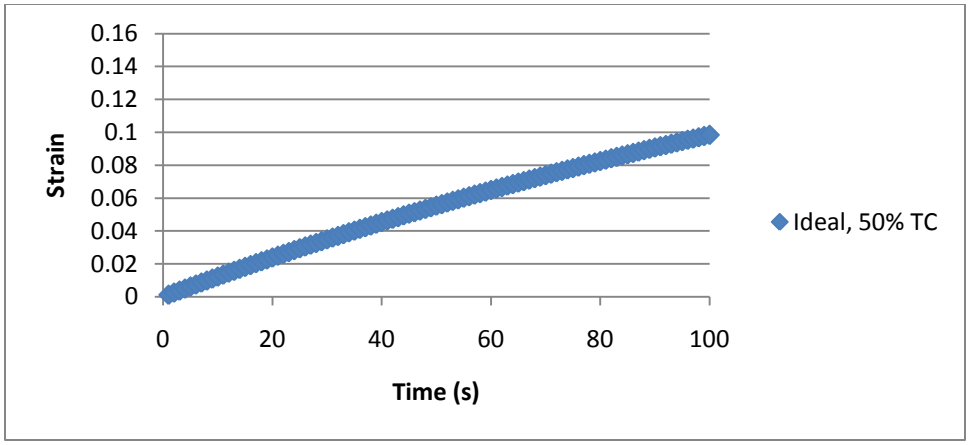

(a)

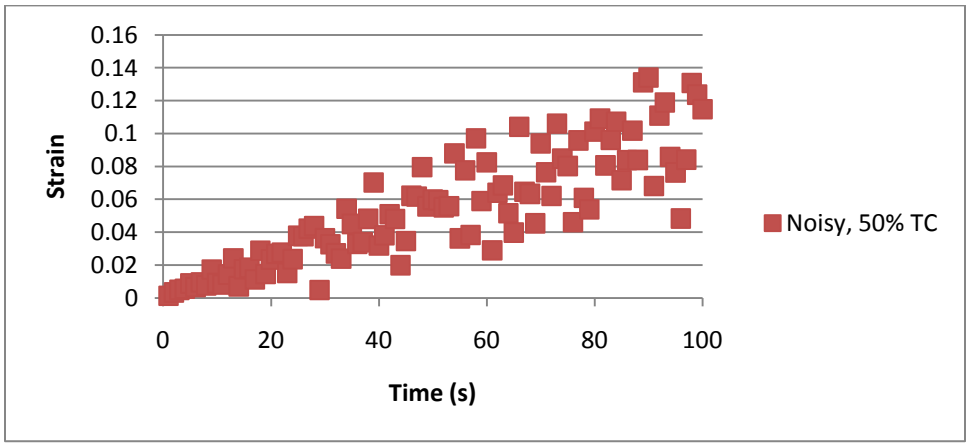

(b)

Figure 3. Example of noisy simulated strain curve. True TC of 200s and acquisition rate of 1 Hz. (a) Ideal curve up to 100 s. (b) Noisy curve obtained from a) after adding noise.

Once 50 TC estimates have been obtained, the accuracy of the estimator is measured. To assess accuracy, the mean absolute error was measured, computed from the absolute error of each of the 50 estimates. Mean absolute error is defined as:

$$Mean\ Absolute\ Error\ (\%) = mean\left(\frac{|(\hat{\tau}_i)-\tau|}{\tau}\right) \cdot 100 \tag{3.1}$$

Another measure considered for error analysis is the bias, given by:

$$Bias\ (\%) = \left(\frac{|mean\ (\hat{\tau}_i)-\tau|}{\tau}\right) \cdot 100 \tag{3.2}$$

The threshold window of observation for a TC is defined as the smallest window of observation, such that, for all windows with equal or longer acquisition time, the accuracy of the LM estimator is always greater than 90%. By observing the error associated with different windows of observation, a threshold window of observation can be determined for a single TC. This process can then be repeated for multiple time constants. The effect of other acquisition parameters, such as acquisition rate and input SNR, can be observed by running multiple simulations (with varying acquisition rates and input SNR) over the same range of time constants.

In addition to the threshold window of observation, two other measures were used for analysis. One of these measures is the total acquisition time necessary for a TC, which is found by simply multiplying the threshold window by the TC:

$$Total\ Acquisition\ Time\ (s) = \left(\frac{Threshold\ Window}{100}\right) \cdot \tau \tag{3.3}$$

This value is useful because it gives a simple, and potentially practical, estimate of the time necessary to accurately estimate a TC under a specific set of acquisition parameters. The other parameter is the output SNR, which can be calculated as:

$$SNR = 20log_{10}\left(\frac{mean\ (\hat{\tau}_i)}{std\ (\hat{\tau}_i)}\right) \tag{3.4}$$

The simulations in the work tested a range of true time constants from 5 to 300 seconds, in increments of 5 seconds. These values are representative of the time

constants expected in some tissues (Qui et al. 2008; Righetti et al. 2007c). Additionally, this range covers some of the time constants that can be expected in tissue-mimicking phantoms, which were used for the experiments considered in this thesis (Righetti et al. 2004; Righetti et al. 2005a; Berry et al. 2006; Wu 2001). Several simulations were done to observe the effect of input SNR and acquisition rate on the threshold window of observation. Table 1 summarizes the simulation parameters used for this study. Note that time constants were tested in increments of 5 seconds, and the ideal values of α and η used are as previously specified.

Table 1. Simulation parameters.

Minimum TC	**Maximum TC**	**SNR (dB)**	**Acquisition rate (Hz)**	**Largest window of observation (% TC)**
5	300	10	100	250
5	300	15	100	140
5	300	20	100	140
5	300	25	100	140
5	300	30	100	140
5	300	30	20	140
5	300	30	2	140

These simulations can be used to test the hypothesis of this work, i.e., that the window of observation necessary for accurate TC estimation depends on the underlying TC. These simulations can also be used to test the possibility of obtaining accurate TC estimates when using acquisition times significantly smaller than the true TC, as well as the effects of input SNR and acquisition rate on the accuracy of the estimates.

2. Simulation results

Figure 4 shows the absolute error of a single TC estimate as a function of the window of observation for 5 different true time constants. An input SNR of 20dB and an acquisition rate of 100 Hz was assumed for this simulation. Statistical analysis of the simulation data reported in Figure 4 suggests that the threshold window of observation for a TC of 300 seconds is close to 15-20% of the TC, whereas the threshold for a TC of 5 seconds is close to 65-75% of the TC. This suggests that the threshold window of observation is a function of the true TC. The results in Figure 4 also suggest that for an equivalent window of observation length (in terms of the percentage of the true TC), smaller time constants generally exhibit higher error than larger time constants. This may be due to the fact that, for these true TC values, there are an insufficient number of data points for the estimator to make a reasonable estimate.

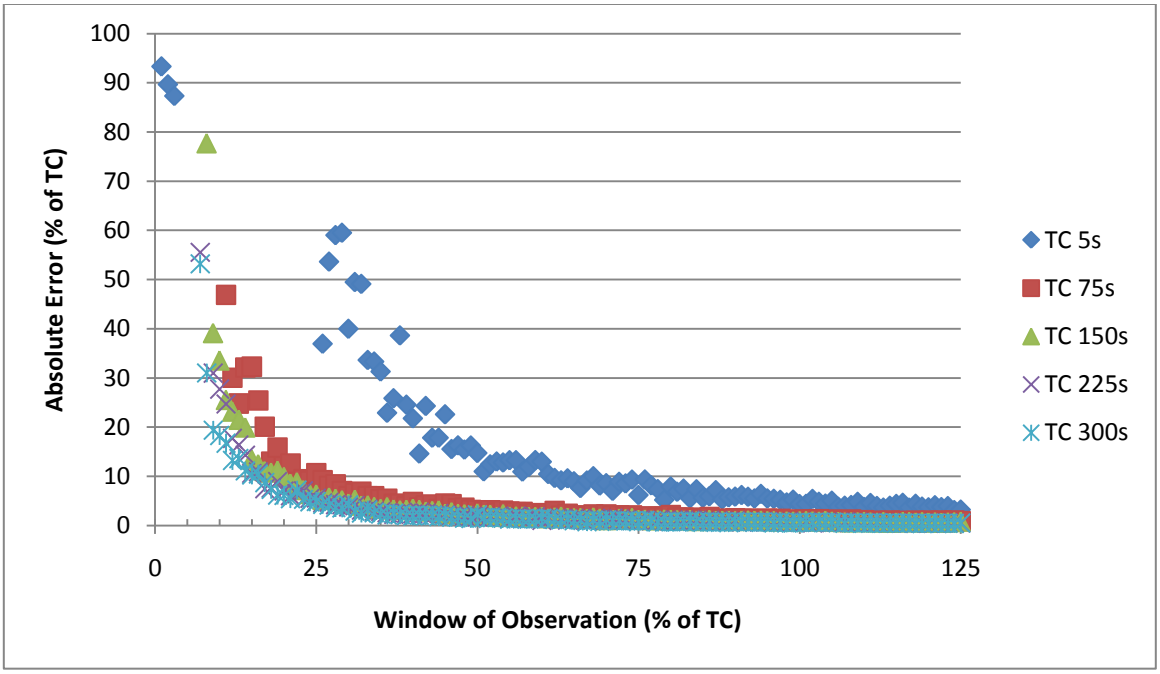

Figure 4. Absolute error of TC estimation vs. window of observation. Input SNR of 20dB and acquisition rate of 100 Hz acquisition rate.

Figure 5 shows the effect of input SNR on the error of a single TC estimate at different acquisition times for a true TC of 150 seconds, an acquisition rate of 100 Hz, and 3 different input SNR levels. The threshold window for 10dB input SNR is close to 40%, whereas the threshold window for 20dB and 30dB input SNR is much lower, around 20% and 10%, respectively. This suggests that input SNR has a significant impact on the threshold window of observation.

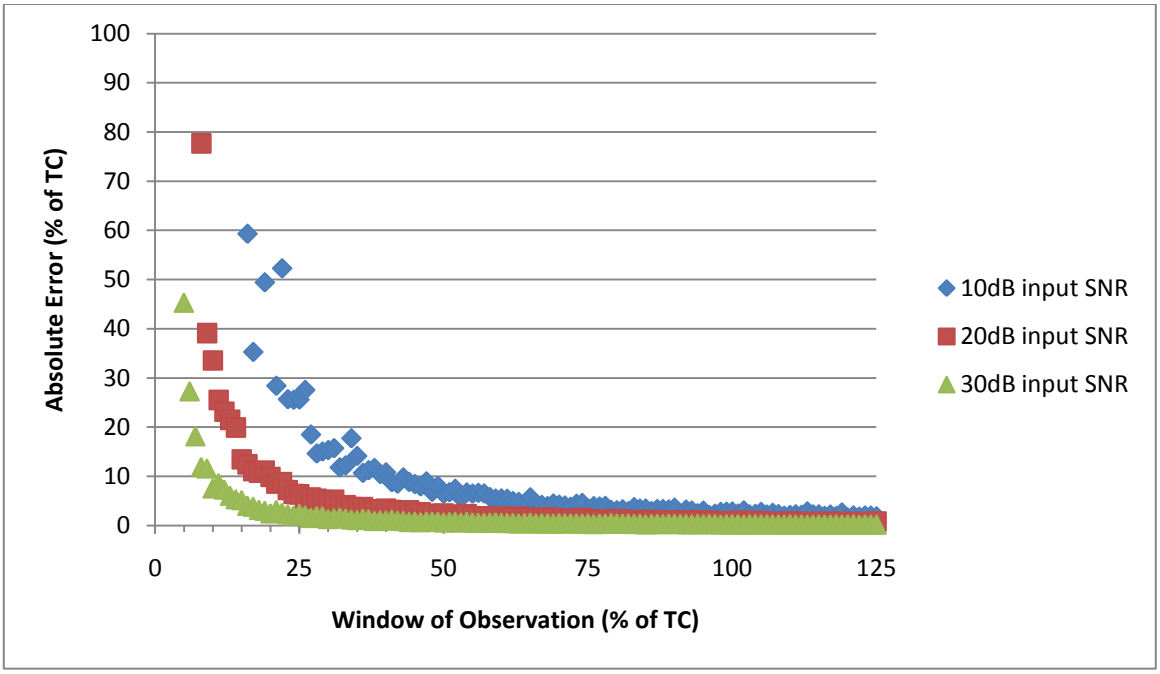

Figure 5. Absolute error of TC vs. window of observation - effect of input SNR. Time constant of 150s and 100 Hz acquisition rate.

Figure 6 shows the effect of acquisition rate on the error of a single TC estimate at different windows of observation for a true TC of 150 seconds, input SNR of 30dB, and 3 different acquisition rates. The threshold window of observation tends to decrease as the acquisition rate increases, suggesting that the threshold window of observation depends on the acquisition rate.

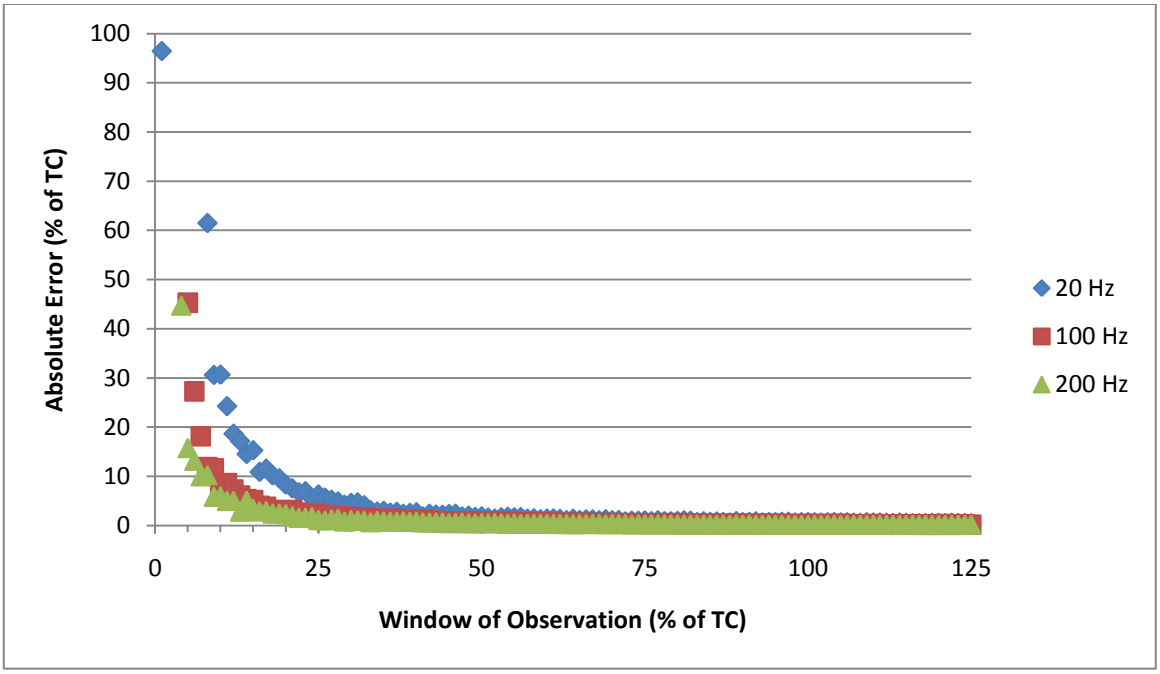

Figure 6. Absolute error of TC vs. window of observation - effect of acquisition rate. Time constant of 150s and input SNR of 30dB.

Figures 7-9 show the error obtained using 4 different error measures as a function of the threshold window of observation at 3 different input SNR levels. 50 estimates were made for the TC at each window of observation. For each window of observation, these figures show the 5th percentile, 95th percentile, median, and mean absolute errors. A TC of 150 seconds was used with an acquisition rate of 100 Hz. The figures show that the mean absolute error and median absolute errors behave similarly at longer windows of observation, regardless of input SNR. Note that windows of observation where the mean error is significantly different from the median error typically correspond to an absolute error greater than 40%, meaning that any outliers from the TC estimation process will not have a significant impact on the calculation of

the threshold window of observation. This justifies the use of the mean absolute error for threshold window of observation calculations. While the mean absolute error is the primary measure used in this study, use of the 95th percentile error may provide a more conservative estimate for the necessary window of observation, especially at lower levels of input SNR, such as the 10dB case. This may be especially useful for experimental work and clinical applications.

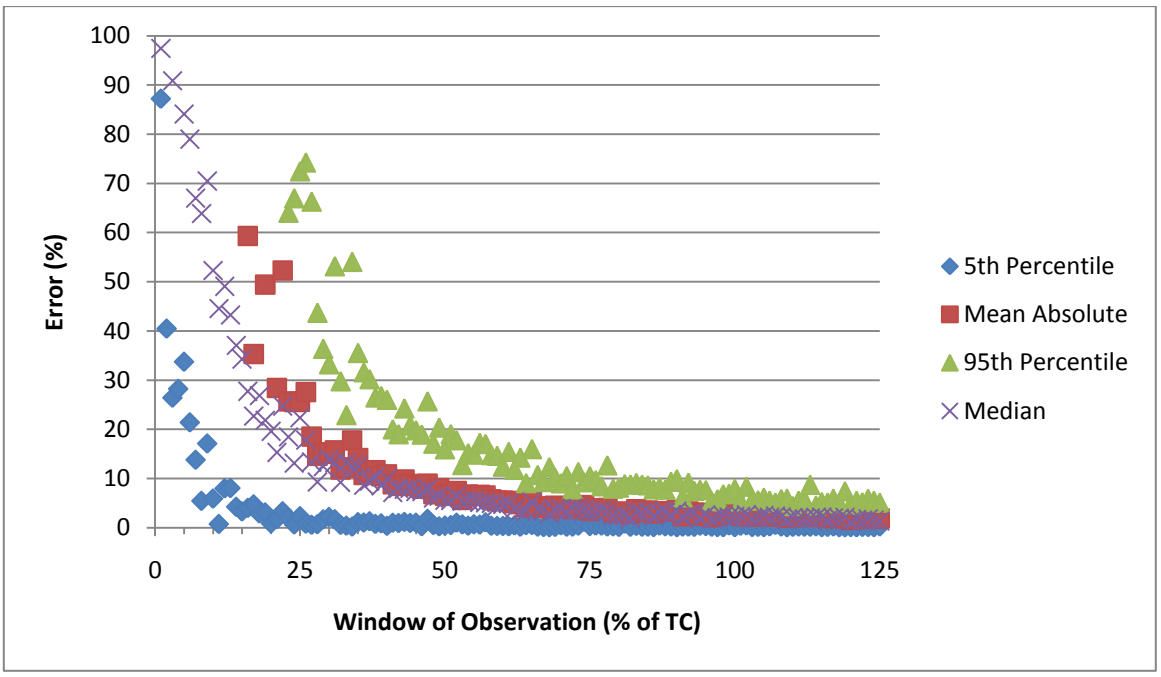

Figure 7. Error measures – 10dB input SNR. TC of 150s and acquisition rate of 100 Hz.

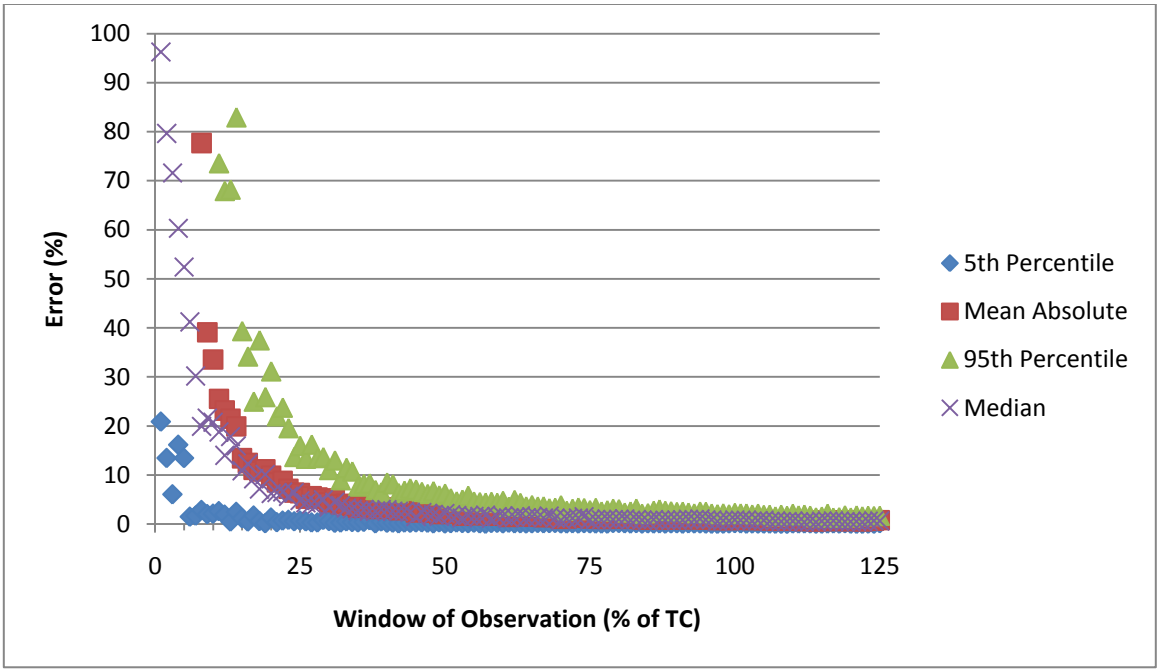

Figure 8. Error measures – 20dB input SNR. TC of 150s and acquisition rate of 100 Hz.

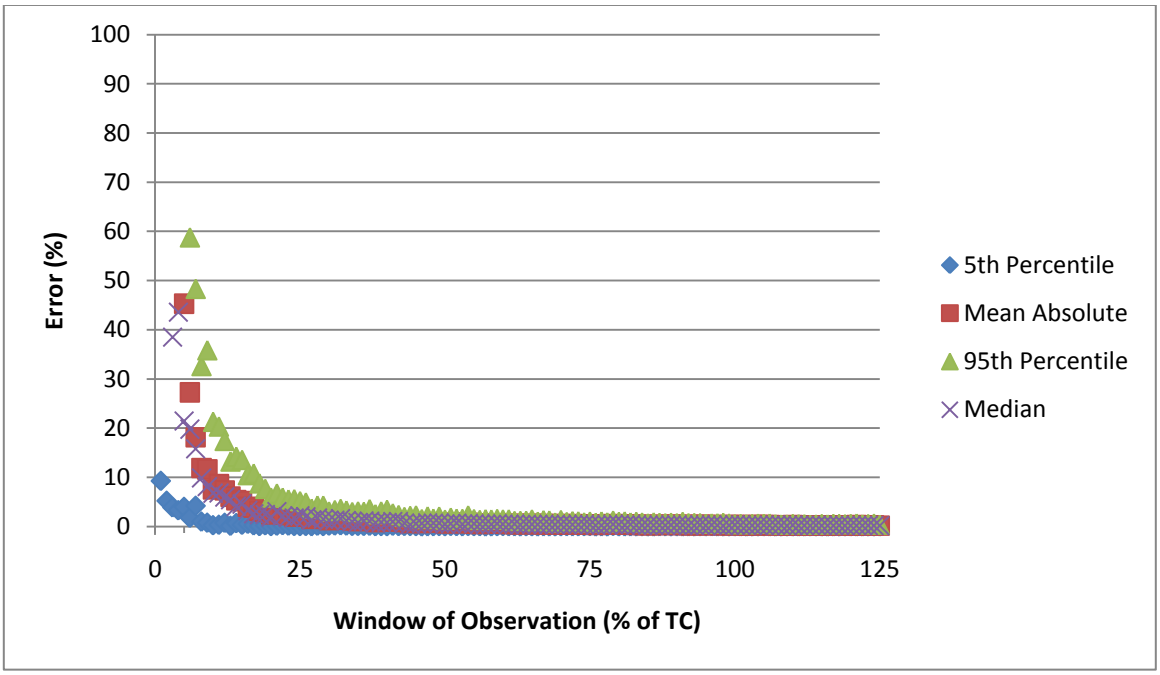

Figure 9. Error measures – 30dB input SNR. TC of 150s and acquisition rate of 100 Hz.

Bias was also considered as an error measure. Figure 10 shows the threshold window of observation as a function of the true TC when the bias and mean absolute error are used. An acquisition rate of 100 Hz with a 20dB input SNR was used for this simulation. Clearly, both measures result in similar trends; however, the threshold determined through the use of the mean absolute error is consistently a more conservative measure than the threshold determined through the use of the bias.

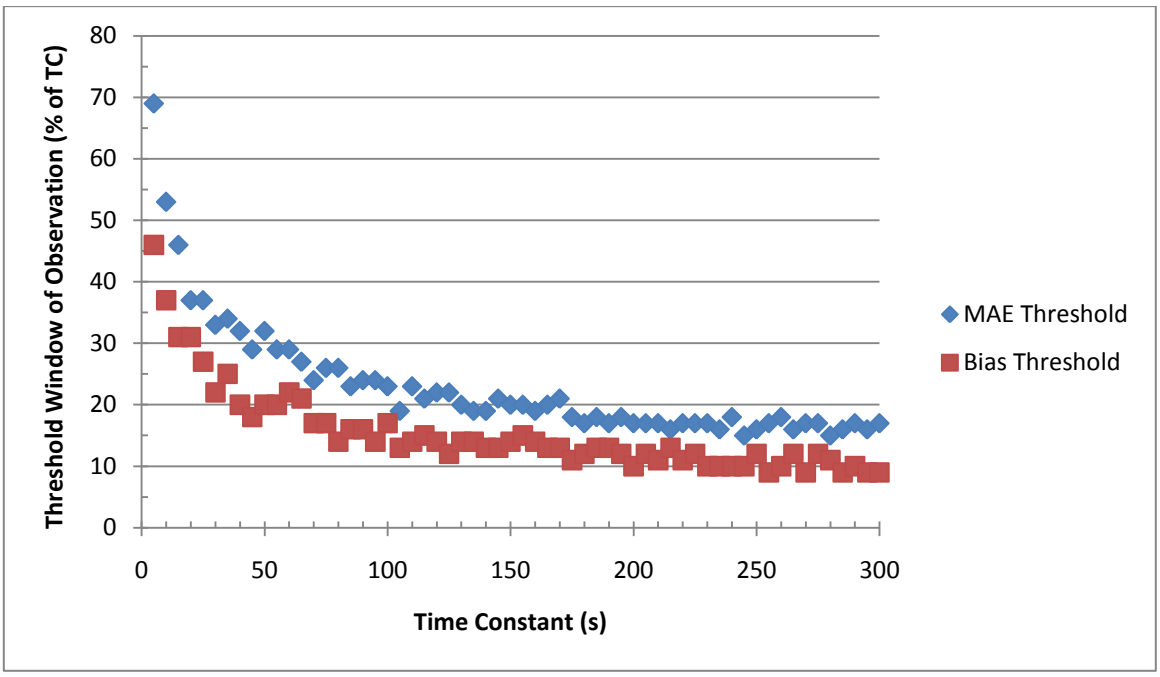

Figure 10. MAE vs. Bias threshold window of observation. Input SNR of 20dB and acquisition rate of 100 Hz.

Figure 11 shows the effect of input SNR on the threshold window of observation for various time constants at an acquisition rate of 100 Hz. As the input noise increases, the estimator requires a larger number of samples (percentage of the TC) to compute an

accurate estimate, especially at small time constant values. Clearly, input noise plays a significant role in the accuracy of the time constant estimator.

Figure 12 shows the effect of acquisition rate on the threshold window of observation for various time constants at an input SNR of 30dB. Figure 12 suggests that acquisition rate can have a significant impact on the amount of time necessary to make an accurate estimate for all TC values used for this study, and especially for short time constants. This is an important observation, which may have implications not only on current ultrasound elastographic techniques, but also on other imaging modalities. For example, the development of ultrafast MR elastography systems may prove to be beneficial for studies aiming at imaging time-dependent phenomena in tissue.

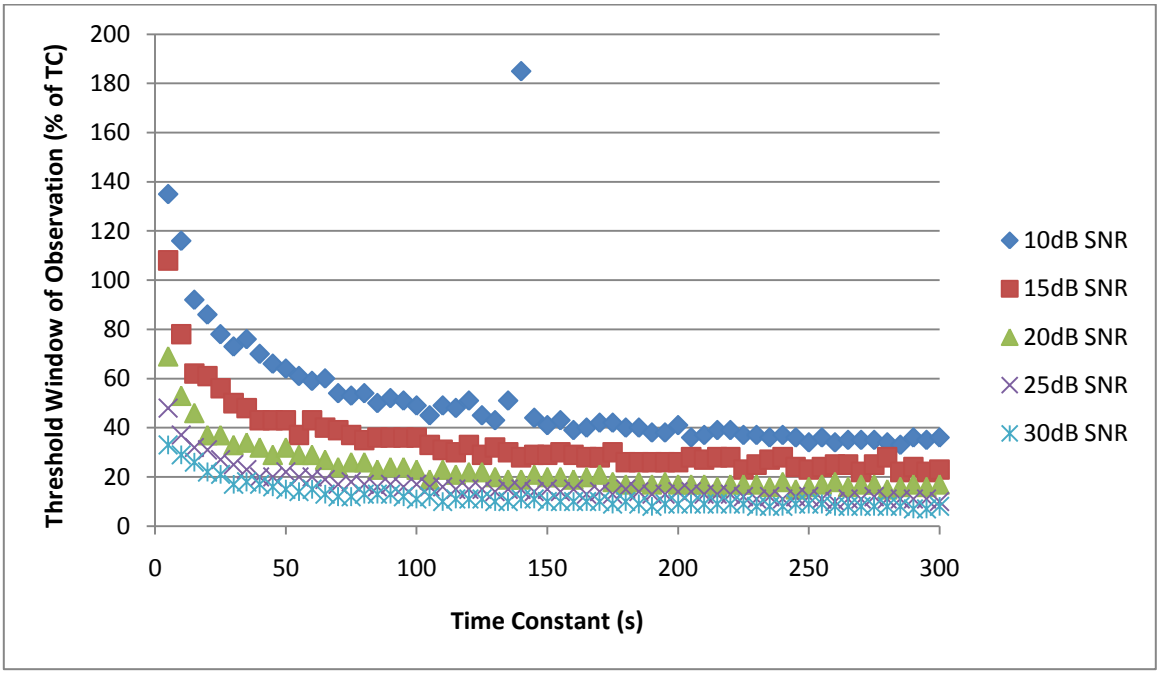

Figure 11. Threshold window of observation vs. TC – effect of input SNR. Acquisition rate of 100 Hz.

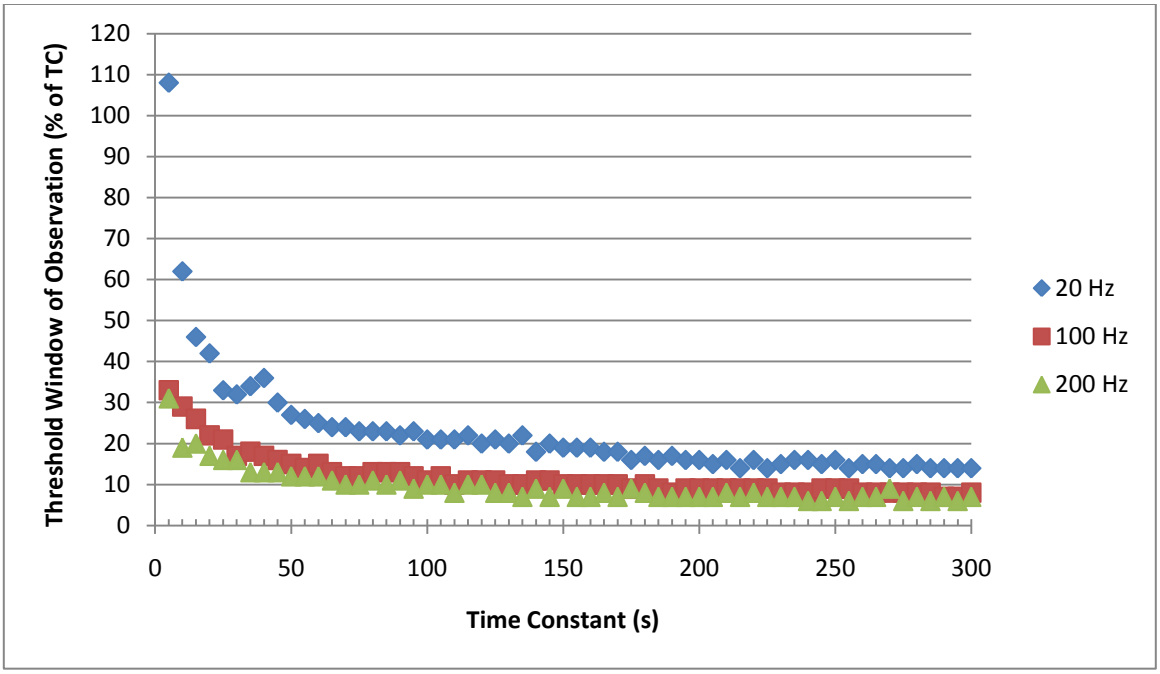

Figure 12. Threshold window of observation vs. TC – effect of acquisition rate. Input SNR of 30dB.

Figures 13 and 14 summarize the simulation results. These graphs give a direct relationship between the total acquisition time necessary for accurate TC estimation and the true TC. Figure 13 shows the total acquisition time from the data in Figure 11, detailing the effect of input SNR on the threshold window of observation. Figure 14 shows the total acquisition time from the data in Figure 12, illustrating the effect of acquisition rate on the threshold window of observation. These figures suggest that there is a linear relationship between the total acquisition time and the underlying TC. The slope of the line describing the relationship depends not only on the input SNR, but also the acquisition rate used. A mathematical model representing this relationship

could be useful for both elastography experiments and clinical applications and is left for future work.

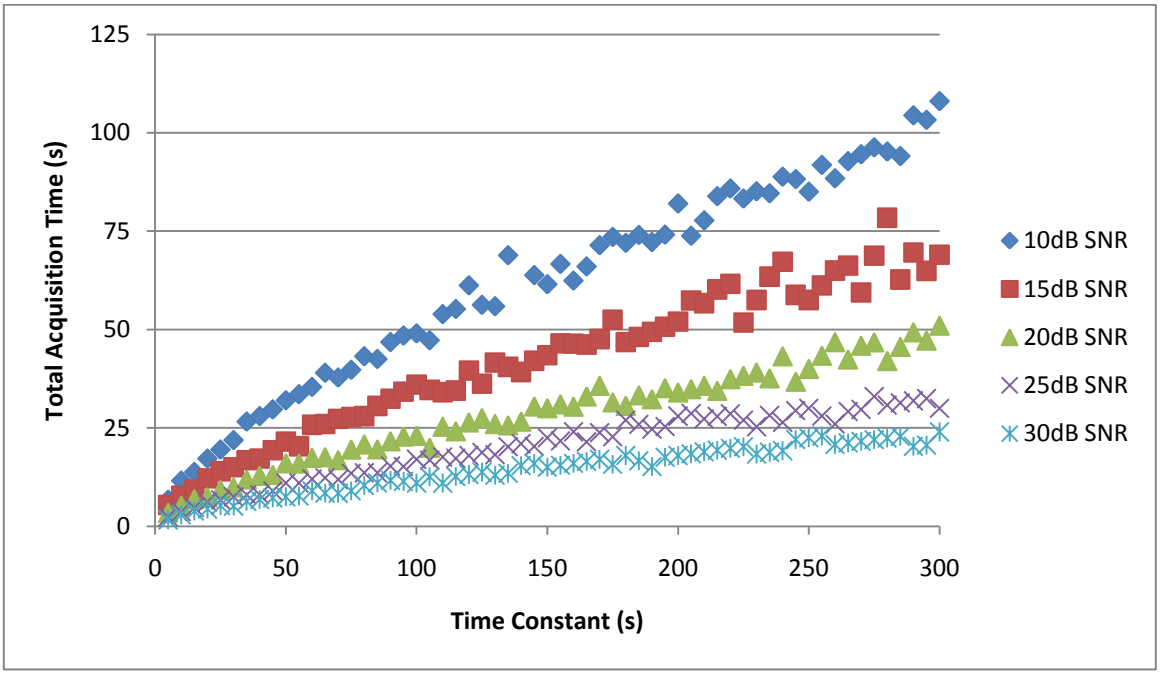

Figure 13. Total acquisition time vs. TC – effect of input SNR. Acquisition rate of 100 Hz.

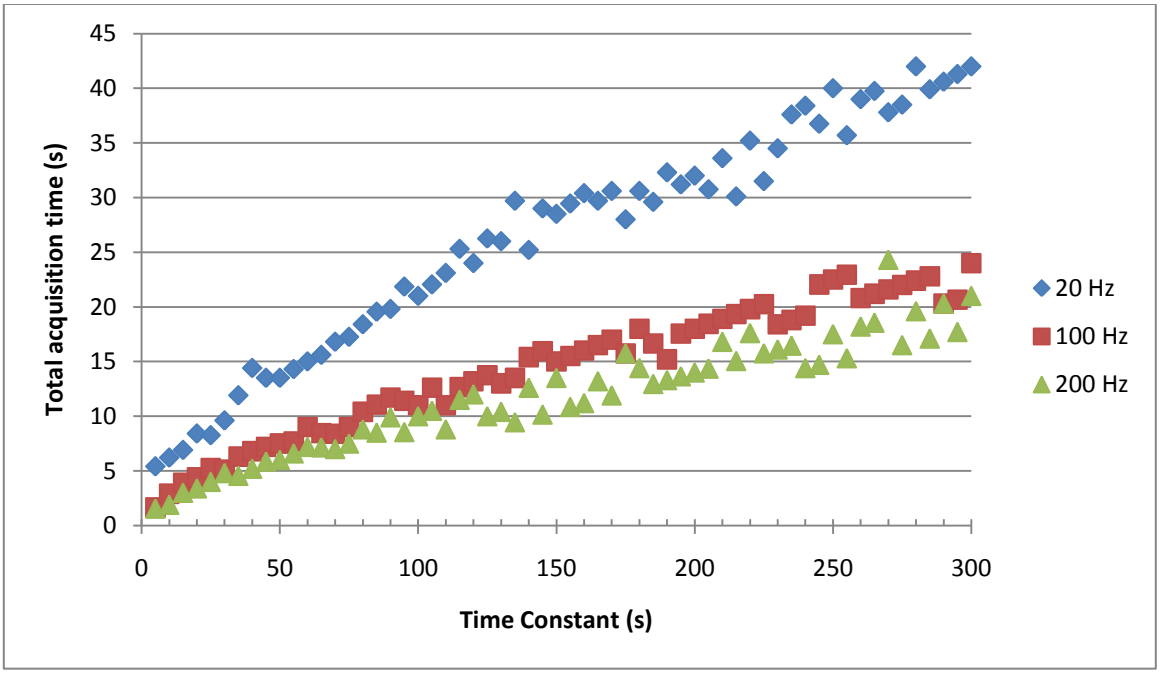

Figure 14. Total acquisition time vs. TC – effect of acquisition rate. Input SNR of 30dB.

A final parameter of interest that can be computed with these simulations is the output SNR. Figures 15-17 show how the expected output SNR varies based on the window of observation used. Output SNR is calculated using equation (3.4). In these graphs, the output SNR obtained when using a collection window equal to the computed threshold is compared to the output SNR for a collection window equal to 100% of the TC. The output SNR when using a window of observation equal to 100% of the TC can be significantly higher than the output SNR obtained when using the threshold window of observation. However, use of the threshold window of observation guarantees at least a 20dB (approximately) output SNR. This result shows that by consistently defining the threshold window of observation length as the minimum window length necessary to

achieve accuracy greater than 90%, we are guaranteed to get a certain level of quality in the output estimates.

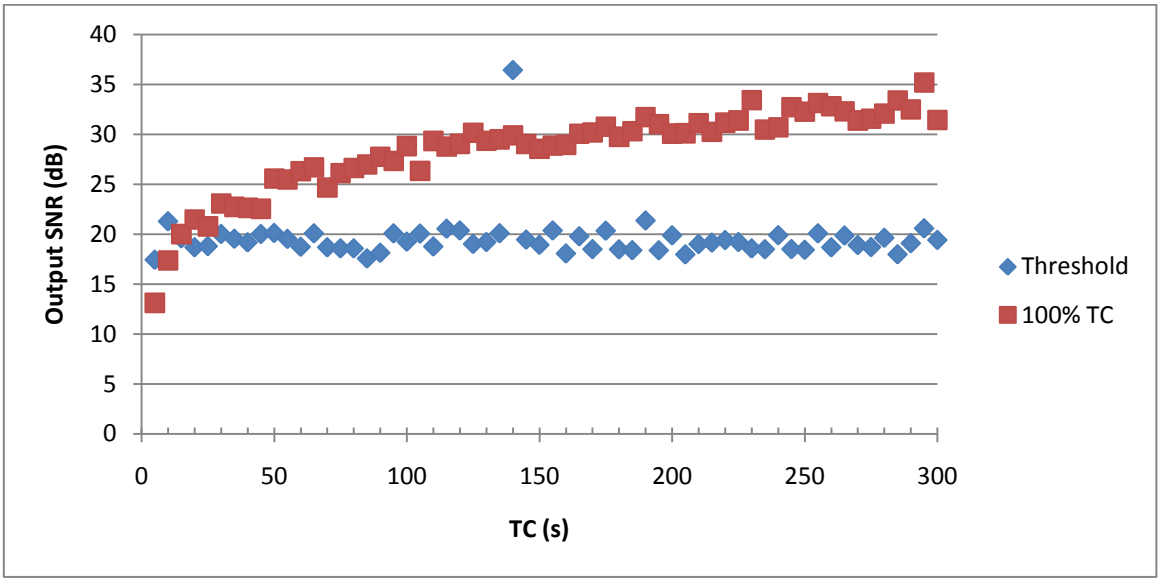

Figure 15. Expected output SNR – 10dB input SNR and 100 Hz acquisition rate.

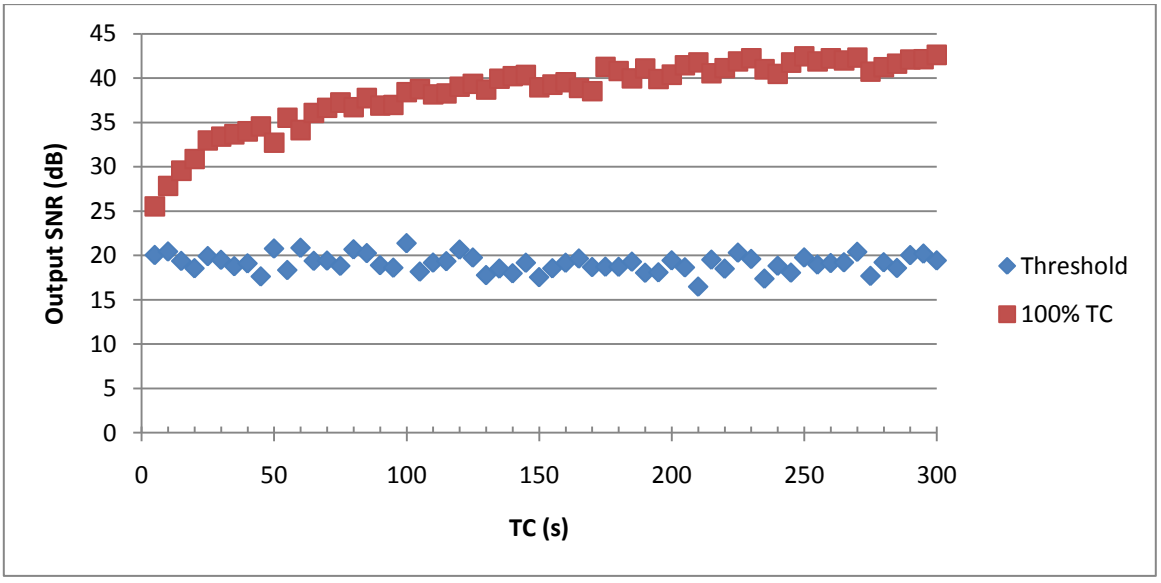

Figure 16. Expected output SNR – 20dB input SNR and 100 Hz acquisition rate.

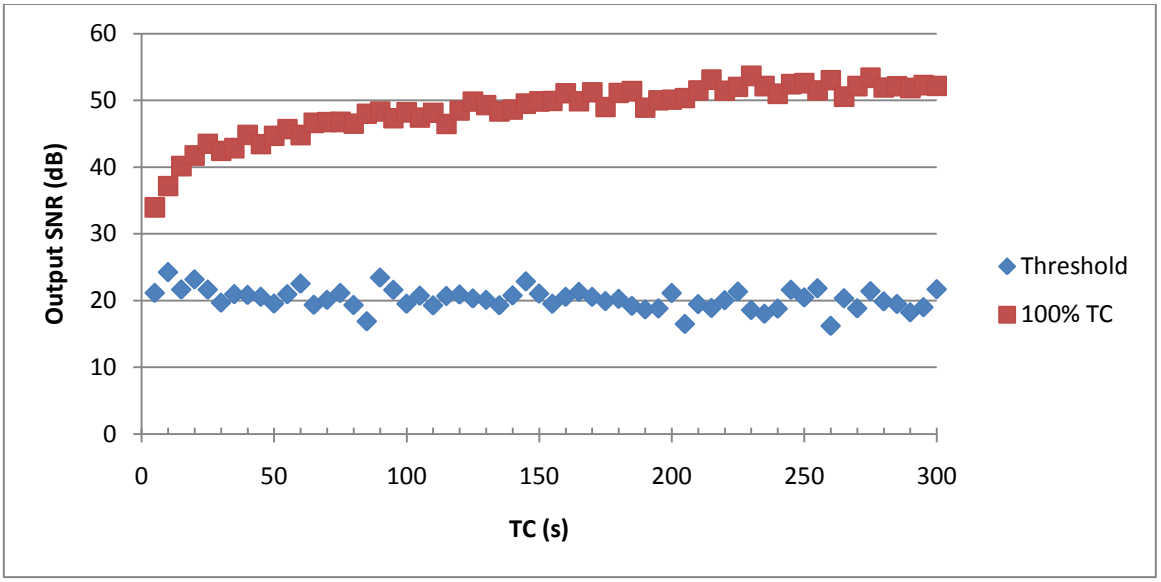

Figure 17. Expected output SNR – 30dB input SNR and 100 Hz acquisition rate.

Note that the expected output SNR obtained when using 100% of the TC collection window increases as the magnitude of the time constant increases, while the expected output SNR obtained when using the threshold window of observation remains practically constant. This is due to the fact that the threshold window of observation length is always the minimum window of observation necessary to achieve accuracy greater than 90%, which guarantees a certain level of quality in the output, and this is reflected in the expected output SNR.

CHAPTER IV

EXPERIMENTAL METHODS AND RESULTS

The experimental results in this work are used to corroborate selected simulation findings and to evaluate the effect of noise sources that are not possible to include in the simulation methods on the predicted threshold window of observation.

1. Experimental methods

The experimental data analyzed in this work was collected in a previous study (Nair 2010; Nair et al. 2011). Briefly, creep tests were performed on three blocks of available tofu, each of them 4 cm thick. Past work has shown that tofu can be used as tissue-mimicking phantom for ultrasound experiments (Righetti et al. 2004; Righetti et al. 2005a; Berry et al. 2006; Wu 2001). Data were acquired using a Sonix RP system (Ultrasonix). The ultrasound transducer was equipped with a custom built compressor plate. The samples were submerged in water and a constant force was applied to the samples using the compressor apparatus (Nair et al. 2011). The transducer used for these experiments was a 38 mm real-time linear array with 128 elements, a bandwidth between 5-14 MHz, a center frequency of 6.6 MHz, 50% fractional bandwidth (at -6 dB), a sampling frequency of 40 MHz, and a 1 mm beamwidth at the focus point.

Each tofu block was submerged in a water bath so that the transducer would be coupled to the tofu. A constant force, replicating the effects of a creep test, was applied to the tofu block through the weight of the transducer, compressor plate, and a sliding

plate. The system collects ultrasound RF frames at specific sample times set by the users. As described in Chapter II, the axial strain $S(t_i)$ is computed in a cumulative manner using consecutive frames to maintain an acceptable correlation level (Nair et al. 2011). Temporal changes in the axial strain distribution can be estimated pixel by pixel. From the temporal curves of the axial strain, the axial strain time constant for each pixel in the elastograms can be computed. A TC elastogram, or a map of the local time constants, can be created for the entire image.

The experimental data presented in this work was collected using an acquisition rate of approximately 1 Hz, which results in a total of 595 frames of RF data. This corresponds to approximately 595 seconds of data. Data could not be collected consecutively at the highest frame rate of the ultrasonic system because the system has a buffer that limits the total number of frames that can be acquired during a single collection. TC elastograms were computed for each tofu block using all 595 frames available. The resulting elastograms were considered to be representative of the true time constants in each block.

This work aims to show that it might be possible to use smaller windows of observation and still estimate the TC with accuracy greater than 90%. To do so, it is necessary to determine the input SNR for each block tested. Ideally, the tofu blocks used in the experiments would be perfectly uniform and the exact time constant of the entire material could be easily determined. Experimental data clearly shows that the tofu blocks used in the experiments are not completely uniform, as expected. Therefore, it is necessary to first pick a representative region of the imaged block, and then select a

representative TC from that region. Figure 18 shows an example of a region chosen as representative of the tofu block imaged.

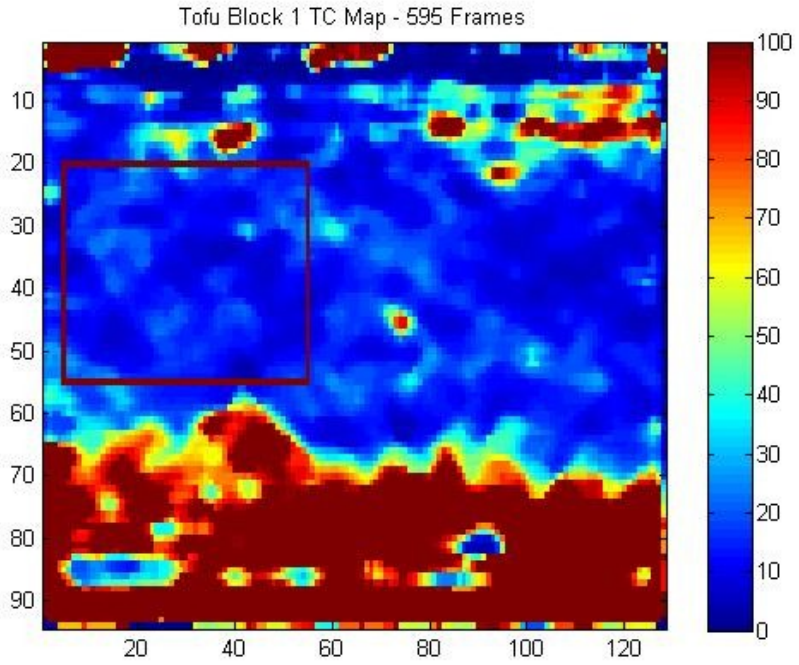

Figure 18. Example of an axial strain TC elastogram from a tofu block. Area within the square indicates the region used for the analysis.

Once a representative region was selected, the true TC of this region was evaluated. The mean TC and the 95th percentile TC in each representative region (from the TC elastograms previously calculated using the entire set of 595 frames) were considered for use in determining a threshold window of observation. The input SNR can then be estimated by computing the SNR of the cumulative axial strain from all 595 frames of data, given by:

$$Input\ SNR = 20log_{10}\left(\frac{mean\ (S_i)}{std\ (S_i)}\right) \quad (4.1)$$

With a known true TC, input SNR, and acquisition rate, a threshold window of observation could be determined through simulations similar to those seen in Chapter III. Therefore, a set of simulations was run to determine the threshold window of observation based on the exact acquisition rate (1 Hz), input SNR, and true TC, as determined from the experimental data. These simulation data were needed to find the predicted threshold window of observation for each experimental set of data. To provide a more conservative estimate of the SNR for each set of experimental data, simulations were run with input SNR levels rounded down to the nearest multiple of 5 dB (10dB and 15dB). The threshold windows of observation for the time constants can be found using the data shown in Figures 19-20. A curve fit using a two exponential model was applied to both cases. This curve fit allows estimation of a threshold window of observation for all time constants less than 2000 seconds.

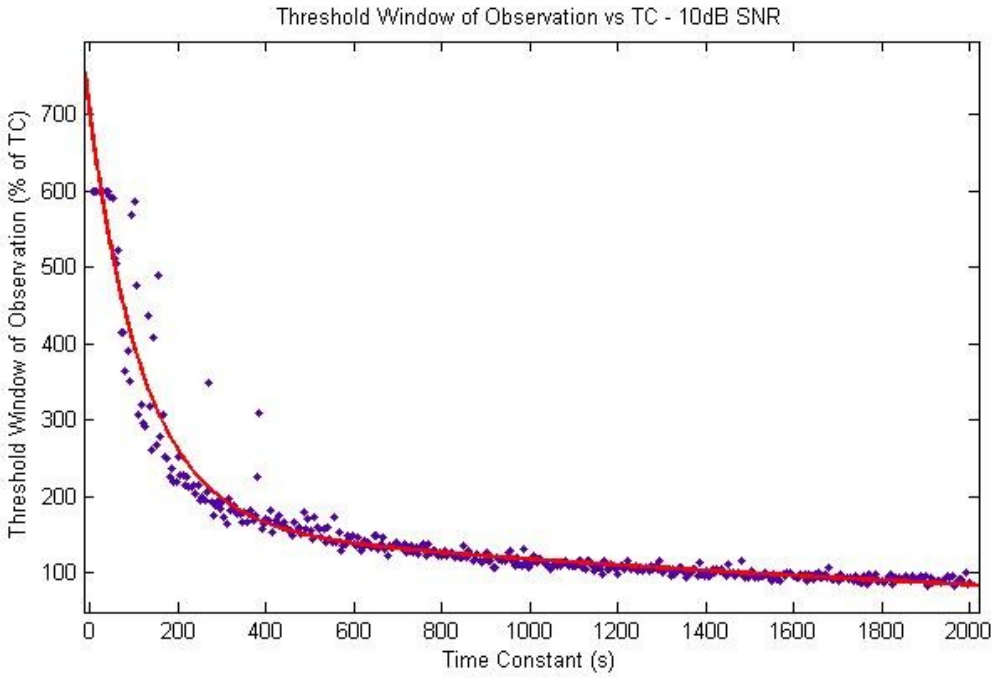

Figure 19. Threshold window of observation vs. TC – 10dB input SNR and 1 Hz acquisition rate.

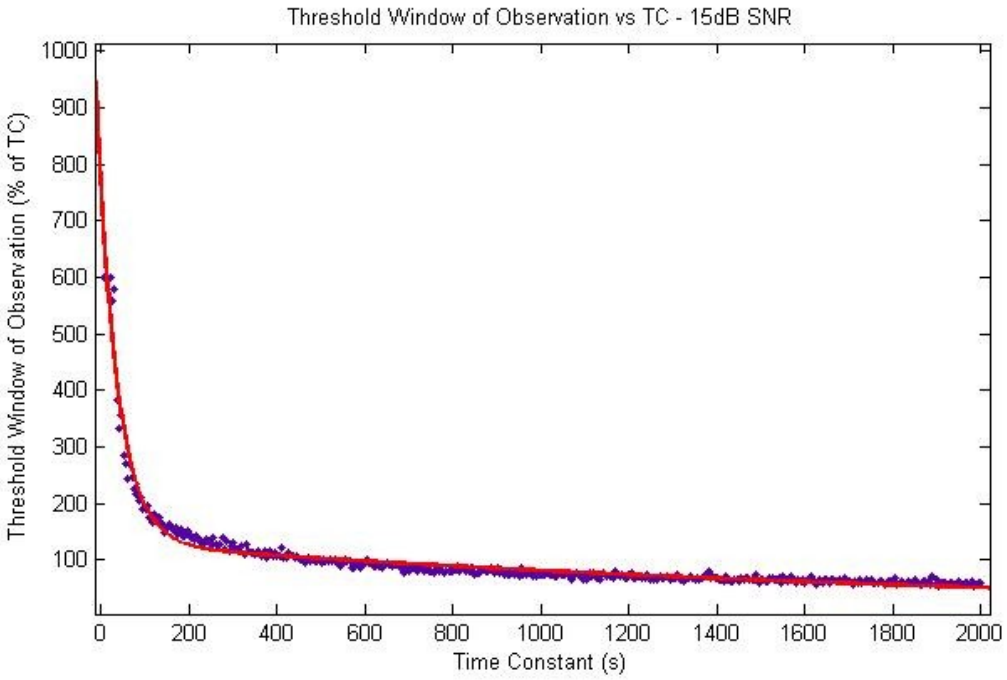

Figure 20. Threshold window of observation vs. TC – 15dB input SNR and 1 Hz acquisition rate.

The curve fit equations for the 10dB and 15dB cases are given by equations (4.2) and (4.3), respectively.

$$T_{10dB}(\tau) = 530.1e^{-.008007\tau} + 164.3e^{-.0003318\tau} \quad (4.2)$$

$$T_{15dB}(\tau) = 608.9e^{-.02137\tau} + 129.9e^{-.0004658\tau} \quad (4.3)$$

Once a threshold window is found, a new TC elastogram can be created by only using the number of frames corresponding to this acquisition time. The new TC elastogram can then be compared with the true TC elastogram in the region of interest, both visually and through computation of the mean absolute error in the region.

Three different tofu blocks were tested. For each region, a threshold window of observation (in seconds) was determined both using the mean TC of the region and the 95^{th} percentile TC of the region. Threshold windows equal to a multiple of the window determined for the mean TC were also tested. This was done because the threshold window determined by simulations should be considered as an optimistic upper bound. In fact, a number of other factors and noise sources may play a role in experimental data, which are not taken into consideration in the simulation model.

2. Experimental results

Figure 18 shows the true TC elastogram for the first tofu block. Table 2 describes the representative parameters of the block, the four threshold windows of the block, and the corresponding errors. Figure 21 shows the true TC map in the selected region and the TC maps obtained when using each of the four threshold windows shown in Table 2.

Table 2. Tofu block 1 parameters.

	Mean TC	95th percentile TC	2x Mean Threshold	3x Mean Threshold
Calculated SNR (dB)	13			
SNR Used (dB)	10			
TC (s)	14	23	---	---
Threshold %	638	606	---	---
Acquisition Time (s)	89	137	178	267
Total Frames	90	139	179	267
MAE (%)	66	60	55	45

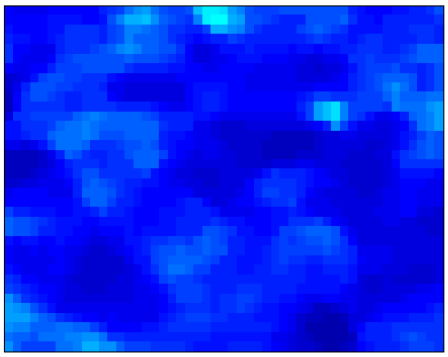

(a)

Figure 21. Tofu block 1 region TC maps. (a) True TC map. (b) TC map using mean TC threshold window. (c) TC map using 95th percentile TC window. (d) TC map using 2x mean TC threshold window. (e) TC map using 3x mean TC threshold window.

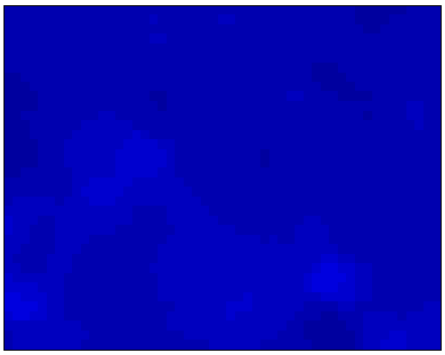

(b)

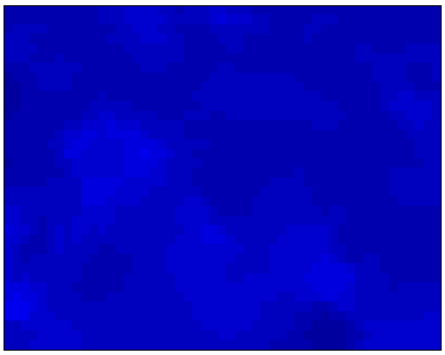

(c)

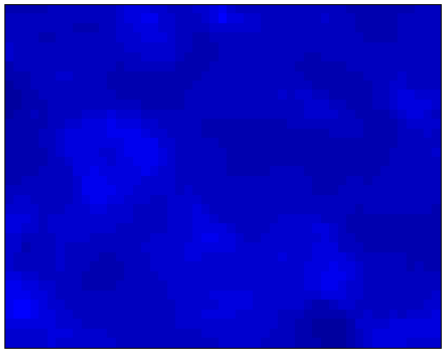

(d)

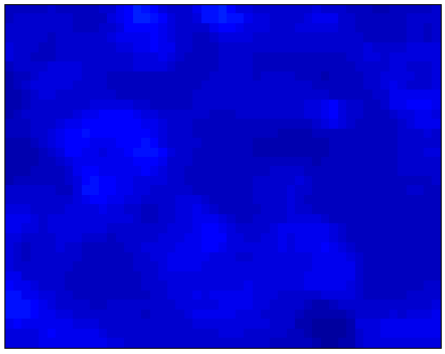

(e)

Figure 21 continued.

Visually, no significant changes appear in the TC maps when using the threshold window of observation (with respect to the true TC map); however, the error analysis shows a MAE > 50% in all cases. This may be due to the fact that the time constants in this block are very small, leading to very large threshold windows of observation, greater than 600% in both cases. In addition, the non-uniformity of the phantom in the selected

area may contribute to the high error. Larger time constants require longer acquisition times, as shown in Chapter III, and may bias the error significantly if present in the selected region. Furthermore, the effect of other sources of noise in experimental data can significantly increase the threshold window of observation. A final factor that makes accurate estimates difficult for this block is the slow acquisition rate. Since the true TC is small, there may simply be too few points for the LM estimator to make accurate estimates of these time constants at smaller windows of observation. The situation may be improved by acquiring frames at a faster rate.

Figure 22 shows the true TC elastogram for tofu block 2. Table 3 shows the representative parameters, threshold windows, and corresponding errors. Figure 23 shows the true TC map in the selected region and the TC maps for the same region when using the four threshold windows shown in Table 3.

The time constants in the second block are larger than those in the previous block, as indicated by a mean TC of 52 seconds and 95^{th} percentile TC of 65 seconds. Computation of the errors using the corresponding threshold windows gives significantly smaller errors (34% and 28%). Larger increases of the window of observation, given by the 1.5x and 2x mean threshold window, significantly reduce the computed error while still reducing the total acquisition time. This indicates that it might be possible to shorten the window of observation and still make accurate estimates of the axial strain TC for experimental data.

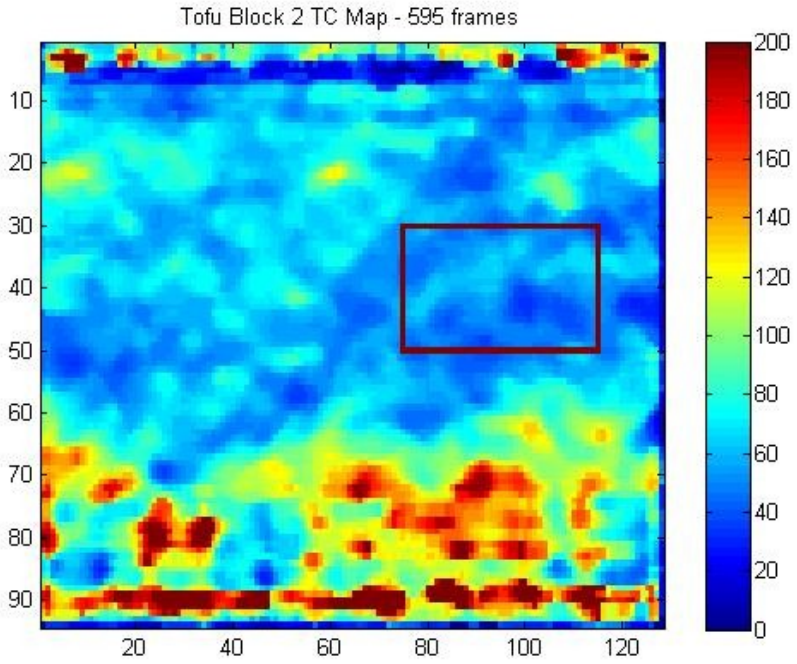

Figure 22. Tofu block 2 true TC map. Area within the square indicates the region used for the analysis.

Table 3. Tofu block 2 parameters.

	Mean TC	95th percentile TC	1.5x Mean Threshold	2x Mean Threshold
Calculated SNR (dB)	14			
SNR Used (dB)	10			
TC (s)	52	65	---	---
Threshold %	513	478	---	---
Acquisition Time (s)	264	308	396	528
Total Frames	265	309	397	529
MAE (%)	34	28	21	11

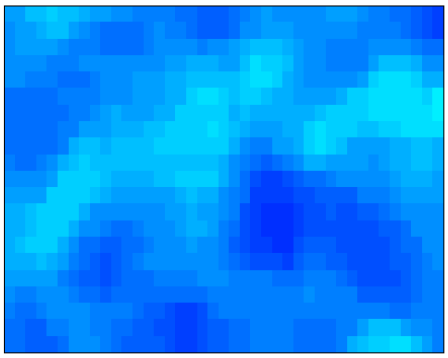

(a)

Figure 23. Tofu block 2 region TC maps. (a) True TC map. (b) TC map using mean TC threshold window. (c) TC map using 95th percentile TC window. (d) TC map using 2x mean TC threshold window. (e) TC map using 3x mean TC threshold window.

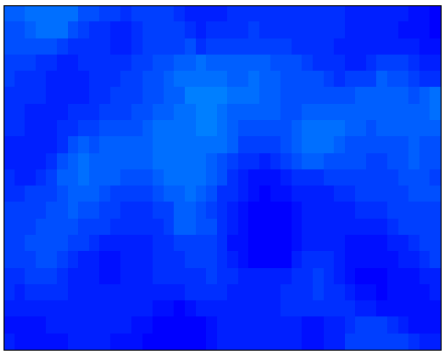

(b)

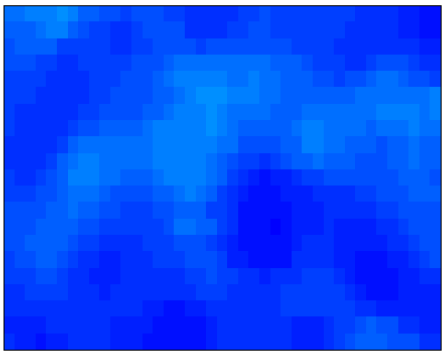

(c)

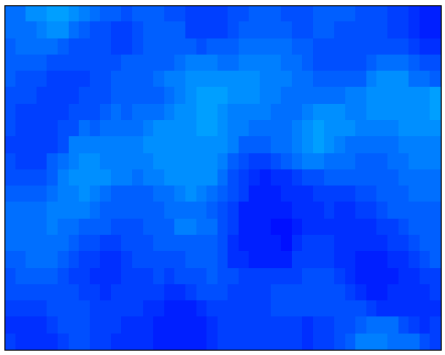

(d)

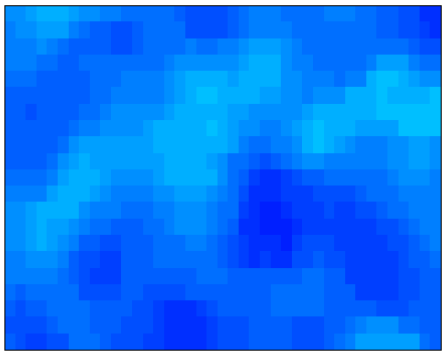

(e)

Figure 23 continued.

Figure 24 shows the true TC elastogram for the third tofu block Table 4 shows the representative parameters, threshold windows, and corresponding errors for tofu block 3. Figure 25 shows the true TC map in the selected region and the TC maps for the same region when using the four threshold windows shown in Table 4.

This block has larger time constants, in the range of 120-150 seconds. Repeating the procedure from the previous blocks again yields a reduction of the error while reducing the total acquisition time. The results from the data again indicate that it might be possible to use relatively short windows of observation and still make accurate estimates of the axial strain TC even in experimental data.

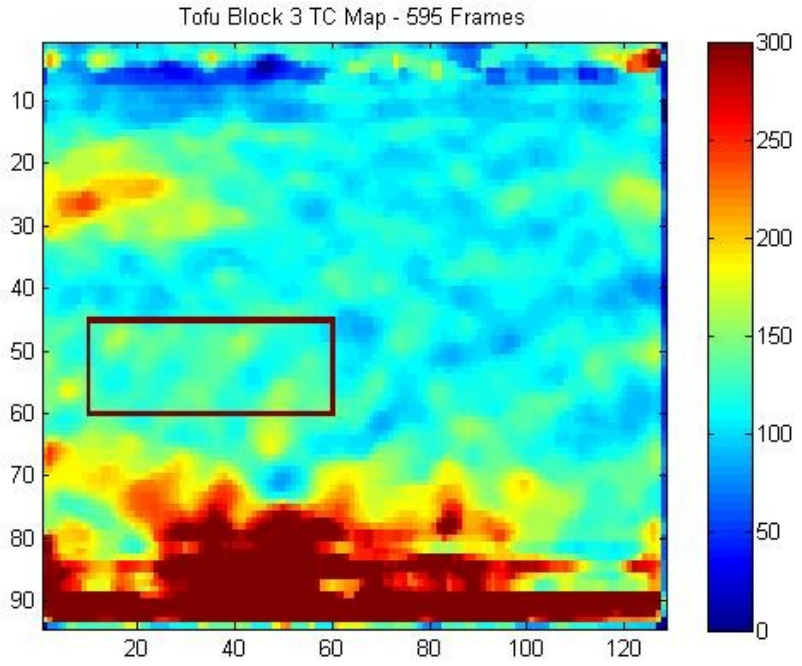

Figure 24. Tofu block 3 true TC map. Area within the square indicates the region used for the analysis.

Table 4. Tofu block 3 parameters.

	Mean TC	95th percentile TC	1.5x Mean Threshold	2x Mean Threshold
Calculated SNR (dB)	19			
SNR Used (dB)	15			
TC (s)	130	151	---	---
Threshold %	161	146	---	---
Acquisition Time (s)	208	219	312	416
Total Frames	209	221	313	418
MAE (%)	39	39	36	19

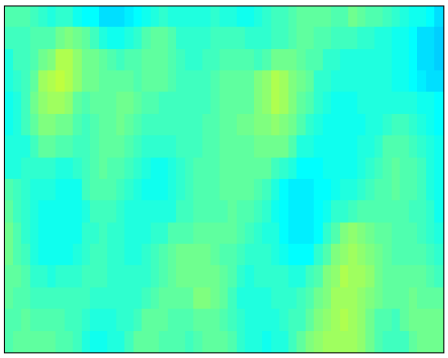

(a)

Figure 25. Tofu block 3 region TC maps. (a) True TC map. (b) TC map using mean TC threshold window. (c) TC map using 95th percentile TC window. (d) TC map using 2x mean TC threshold window. (e) TC map using 3x mean TC threshold window.

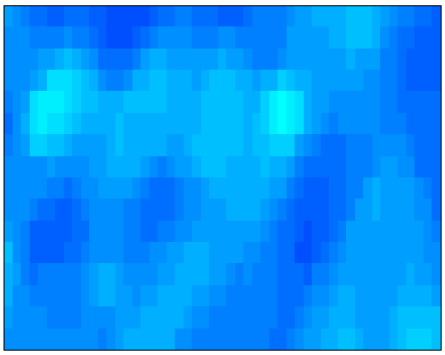

(b)

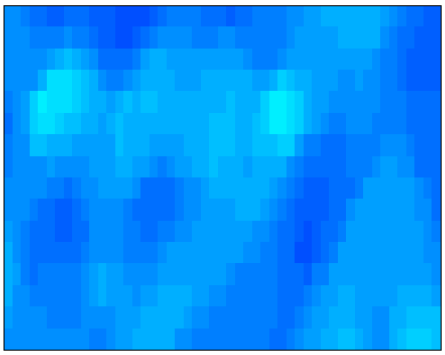

(c)

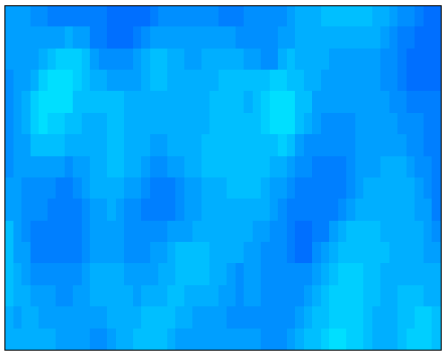

(d)

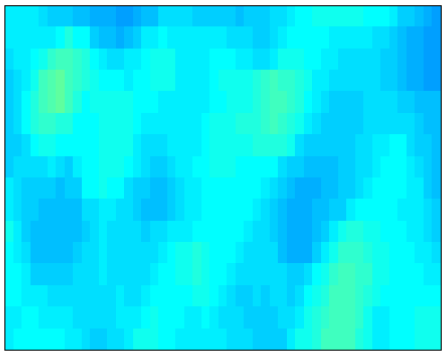

(e)

Figure 25 continued.

CHAPTER V

CONCLUSION AND FUTURE WORK

1. Conclusion

The simulation study performed in this work confirmed the original hypothesis that the total acquisition time necessary for accurate TC estimates depends on the underlying time constant value. The results of the simulations suggest that there is a linear dependence of the total acquisition time for accurate estimates on the true time constant value. Simulations also showed that accurate estimates of the axial strain TC could be achieved with windows of observation shorter than the true TC with fast acquisition rates. Experimental data confirmed that it might be possible to shorten the window of observation for TC elastography without significantly reducing TC estimate accuracy. These results could have important practical implications in elastographic studies that aim at imaging the temporal behavior of tissues.

Additionally, the results of this work suggest that the minimum window of observation necessary for an accurate TC estimate is highly dependent on the acquisition frame rate. Therefore, the use of imaging systems with fast acquisition rates is strongly recommended for studies aiming at measuring tissue time-dependent phenomena.

2. Future work

Estimation of equilibrium strain

The TC estimator used in this work estimates both the TC and the equilibrium strain value of an axial strain curve, which are unknown from noisy strain samples (Nair et al. 2011). While the scope of this work was limited to the study of the effects of acquisition parameters on TC estimation, a similar study of the effect of temporal acquisition parameters on equilibrium strain estimation may be useful. The equilibrium point of the strain is highly dependent on tissue fluid content and mobility, and may also yield important diagnostic information (Righetti et al. 2007b; Nair et al. 2011).

Experimental validation

The experimental data presented in this study is offered as a proof of concept. The relationship between the threshold window of observation, the underlying TC of a material, and the effects of acquisition parameters needs to be studied and corroborated with more experimental data.

Creation of mathematical model for acquisition time

As discussed in Chapter III, the total acquisition time for an accurate TC estimate depends on the acquisition rate and the input SNR. The creation of a mathematical model for the total acquisition time necessary for accurate estimates could be very useful to automatically predict the required threshold window of observations while performing an experiment.

Ideally, the findings of this study could be translated into a simple tool that could be used by a physician or ultrasound technician to quickly determine how long elastography data should be acquired in a clinical application. Creation of a database with the expected time constants of various materials, such as tumors, soft tissues, and muscles, would be the first step toward this goal. This database could be used in conjunction with the mathematical model for total acquisition time to provide practical acquisition times for several clinical applications.

Applications to other time-dependent phenomena in tissues

The temporal behavior of the EPR of a material can contain important information about a tissue state. Under certain assumptions, the strain model used in this work may also be used to approximate EPR temporal behavior (Righetti et al. 2007b; Nair et al. 2011). Therefore, the use of smaller windows of observation and faster acquisition rates may be beneficial for EPR TC elastograms. The results of this work may also be useful for time-dependent phenomena with modalities other than ultrasound, such as MR elastography.

REFERENCES

Ammann JJ, Rivera R, Ophir J. Rheological modeling of the time-dependent behavior of poroelastic materials under creep test experiments. 5th International Conference on the Ultrasonic Measurement of Tissue Elasticity, Snowbird, UT, October 8-11, 2006.

Armstrong CG, Lai WM, Mow VC. An analysis of the unconfined compression of articular cartilage. J Biomech Eng 1984; 106: 165-173.

Bendat JS, Piersol AG. Random data. Analysis and measurements procedures. New York: John Wiley and Sons, 1986.

Berry GP, Bamber JC, Armstrong CG, Miller NR, Barbone PE. Towards an acoustic model-based poroelastic imaging method: I. Theoretical foundation. Ultrasound Med Biol 2006; 32(4): 547-567.

Berry GP, Bamber JC, Mortimer PS, Bush NL, Miller NR, Barbone PE. The spatio-temporal strain response of oedematous and nonoedematous tissue to sustained compression in vivo. Ultrasound Med Biol 2008; 34(4): 617-629.

Cantrell CA. Technical note: Review of methods for linear least-squares fitting of data and application to atmospheric chemistry problems. Atmos Chem Phys 2008; 8: 5477-5487.

Chaudhry A. Performance effect of boundary conditions on performance of poroelastographic imaging techniques in non-homogenous poroelastic media. Master's thesis, Texas A&M University, College Station, TX, 2010.

Collins RE. Flow of fluids through porous materials. New York: Reinhold Publishing, 1961.

Folkman J. The role of angiogenesis in tumor growth. Semin Cancer Biol 1992; 3: 65-71.

Fortin M, Buschmann MD, Bertrand MJ, Foster FS, Ophir J. Dynamic measurement of internal solid displacement in articular cartilage using ultrasound backscatter. J Biomech 2003; 36(3): 443-447.

Fung YC. Biomechanics: Biomechanical properties of living tissues. New York: Springer, 1981.

Itoh A, Ueno E, Tohno E, Kamma H, Takahashi H, Shiina T, Yamakawa M, Matsumura T. Breast disease: Clinical application of US elastography for diagnosis. Radiology 2006; 239(2): 341-350.

Konofagou EE, Harrigan TP, Ophir J, Krouskop TA. Poroelastography: Imaging the poroelastic properties of tissues. Ultrasound Med Biol 2001; 27: 1387-1397.

Liu D, Ebbini ES. Viscoelastic property measurement in thin tissue constructs using ultrasound. IEEE Trans Ultrason Ferroelectr Freq Control 2008; 55(2): 368-383.

Lu JH, Guo ZL, Chai ZH, Shi BC. Numerical study on the tortuosity of porous media via lattice Boltzmann method. Commun Comput Phys 2009; 6: 354-366.

Madsen K, Nielsen NB, Tingleff O. Methods for nonlinear least squares problems. Technical Report. Informatics and Mathematical Modeling: Technical University of Denmark, 2004.

Mridha M, Ödman S. Noninvasive method for assessment of subcutaneous edema. Med Biol Eng Comput 1986; 24: 393-398.

Nair SP. Performance analysis of a new ultrasound axial strain time constant estimation. Master's thesis, Texas A&M University, College Station, TX, 2010.

Nair SP, Yang X, Krouskop TA, Righetti R. Performance analysis of a new real-time elastographic time constant estimator. IEEE Trans Med Imaging 2011; 30(2): 497-511.

Nilsson JW, Riedel SA. Electric circuits. New Jersey: Pearson Prentice Hall, 2005.

Ophir J, Céspedes EI, Ponnekanti H, Yazdi Y, Li X. Elastography: A quantitative method for imaging the elasticity of biological tissues. Ultrason Imaging 1991; 13: 111-134.

Ophir J, Alam K, Garra B, Kallel F, Konofagou EE, Krouskop TA, Varghese T. Elastography: Ultrasonic estimation and imaging of the elastic properties of tissues. Proc Inst Mech Eng H 1999; 1-31.

Qiu Y, Sridhar M, Tsou J K, Lindfors K, Insana M. Ultrasonic viscoelasticity imaging of nonpalpable breast tumors: Preliminary results. Acad Radiol 2008; 15: 1526-1533.

Righetti R, Ophir J, Srinivasan S, Krouskop TA. The feasibility of using elastography for imaging the Poisson's ratio in porous media. Ultrasound Med Biol 2004; 30: 215-228.

Righetti R, Ophir J, Krouskop TA. A method for generating permeability elastograms and Poisson's ratio time-constant elastograms. Ultrasound Med Biol 2005a; 31(6): 803-816.

Righetti R, Ophir J, Garra BS, Chandrasekhar RM, Krouskop TA. A new method for generating poroelastograms in noisy environments. Ultrason Imaging 2005b; 27(4): 201-220.

Righetti R, Srinivasan S, Thitai Kumar A, Ophir J and Krouskop TA. Assessing image quality in effective Poisson's ratio elastography and poroelastography – Part I. Physics Med Biol 2007a; 52: 1303-1320.

Righetti R, Righetti M, Ophir J, Krouskop TA. The feasibility of estimating and imaging the mechanical behavior of poroelastic materials using axial strain elastography. Phys Med Biol 2007b; 52(11): 3241-3259.

Righetti R, Garra BS, Mobbs LM, Kraemer-Chant CM, Ophir J, Krouskop TA. The feasibility of using poroelastographic techniques for distinguishing between normal and lymphedematous tissues in vivo. Phys Med Biol 2007c; 52(21): 6525-6541.

Sack I, Beierbach B, Hamhaber U, Klatt D, Braun J. Non-invasive measurement of brain viscoelasticity using magnetic resonance elastography. NMR Biomed 2008; 21(3): 265-271.

Samarin YP. Construction of exponential approximations for creep curves by the method of successive separation of exponential components. Probl Prochn 1974; 9: 24-27.

Shannon CE. Communication in the presence of noise. Proc Insti Radio Eng 1949; 37(1): 10-21.

Sridhar M, Insana MF. Ultrasonic measurements of breast viscoelasticity. Med Phys 2007; 34(12): 4757-4767.

Sridhar M, Liu J, Insana MF. Viscoelasticity imaging using ultrasound: Parameters and error analysis. Phys Med Biol 2007; 52: 2425-2443.

Srinivasan S, Krouskop TA, Ophir J. Comparing elastographic strain images with modulus images obtained using nanoindentation: Preliminary results using phantoms and tissue samples. Ultrasound Med Biol 2004; 30(3): 329-343.

Thomas A, Kümmel S, Fritzche F, Warm M, Ebert B, Hamm B, Fischer T. Real-time sonoelastography performed in addition to B-mode ultrasound and mammography: Improved differentiation of breast lesions. Acad Radiol 2006; 13: 1496-1504.

Thomas A, Warm M, Hoopmann M, Diekmann F, Fischer T. Tissue Doppler and strain imaging for evaluating tissue elasticity of breast lesions. Acad Radiol 2007; 14: 522-529.

Wu J. Tofu as a tissue-mimicking material. Ultrasound Med Biol 2001; 27: 1297-1300.

Zhang G. Evaluating the viscoelastic properties of biological tissues in a new way. J Musculoskelet Neuronal Interact 2005; 5(1): 85-90

Zhi H, Ou B, Luo BM, Feng X, Wen YL, Yang HY. Comparison of ultrasound elastography, mammography, and sonography in the diagnosis of solid breast lesions. J Ultrasound Med 2007; 26: 807-815.

VITA

Name:	Joshua Kavunkal Varghese
Address:	Department of Electrical and Computer Engineering Texas A&M University 214 Zachry Engineering Center TAMU 3128 College Station, Texas 77843-3128
Email Address:	joshuakvarghese@gmail.com
Education:	B.S., Electrical Engineering, Texas A&M University, 2009